Molecular-beam optical Stark and Zeeman study of the A ^{2}Π--X ^{2}Σ^{+} (0,0) band system of BaF

Timothy C. Steimle, Sarah Frey, Anh Le, David DeMille, David. A. Rahmlow, and Colan Linton

Phys. Rev. A **84**, 012508 — Published 19 July 2011

DOI: 10.1103/PhysRevA.84.012508

A molecular-beam optical Stark and Zeeman study of the $A^2\Pi$-$X^2\Sigma^+$ (0,0) band system of BaF

Timothy C. Steimle*, Sarah Frey and Anh Le
Department of Chemistry and Biochemistry
Arizona State University
Tempe, AZ 85287-1604

David DeMille and David. A. Rahmlow†
Department of Physics
Yale University
PO Box 208120
New Haven, CT 06520

Colan Linton
Centre for Laser Atomic and Molecular Sciences
Physics Department
University of New Brunswick
P.O. Box 4400
Fredericton, New Brunswick, E3B 5A3

Last Modified: May 21, 2011

Send Proofs to: Prof. T. C. Steimle, Department of Chemistry and Biochemistry, Arizona State University, Tempe, Arizona 85287-1604
†Current Address:
Department of Physics, University of Connecticut, 2152 Hillside Road, U-3046 Storrs, CT 06269-3046

- e-Mail: Tsteimle@ASU.edu

Abstract

The $A^2\Pi$-$X^2\Sigma^+$ (0,0) band system of barium monofluoride (BaF) has been recorded using high-resolution laser-induced fluorescence spectroscopy both field-free and in the presence of a static magnetic and electric fields. The field-free spectra for the ^{135}BaF, ^{137}BaF and ^{138}BaF isotopologues were modeled to generate an improved set of spectroscopic constants for the $A^2\Pi(\upsilon=0)$ and $X^2\Sigma^+(\upsilon=0)$ states. The observed optical Stark shifts for the ^{138}BaF isotopologue were analyzed to produce the permanent electric dipole moments of 1.50(2) D and 1.31(2) D for the $A^2\Pi_{1/2}(\upsilon=0)$ and $A^2\Pi_{3/2}$ ($\upsilon=0$) states, respectively. The observed optical Zeeman shifts for the ^{138}BaF isotopologue were analyzed to produce a set of magnetic g-factors for the $A^2\Pi(\upsilon=0)$ and $X^2\Sigma^+(\upsilon=0)$ states.

I. INTRODUCTION

There is renewed interest in measuring and predicting the properties of barium monofluoride, BaF, because of its use as a sensitive experimental venue for quantification of *P*- and *P*,*T*-odd effects [1-9]. The determination of the electric dipole moment (EDM) of the electron, d_e, provides insight into the violation of parity inversion symmetry (*P*) and time-reversal invariance (*T*). Such effects are nuclear spin independent and studies of both the even and odd BaF isotopologues are relevant. The interaction of the nuclear anapole moment, a *P*-odd magnetic moment induced by weak interactions within the nucleus, with the spin of the penetrating nucleus is a nuclear spin dependent parity violation effect. This latter interaction can be probed via studies of only the odd BaF isotopologues. The effective Hamiltonian operator for the $X\,^2\Sigma^+$ electronic state of BaF, including the PNC relevant terms, is [1,9]:

$$\begin{aligned}\mathbf{H}^{eff}(^2\Sigma) &= B\mathbf{N}^2 + \gamma\mathbf{N}\cdot\mathbf{S} + b_F\mathbf{I}\cdot\mathbf{S} + c(I_zS_z - \tfrac{1}{3}\mathbf{I}\cdot\mathbf{S}) \\ &+ eq_0Q\frac{3I_z - \mathbf{I}^2}{4I(2I\text{-}1)} + W_Ak_A\mathbf{n}\times\mathbf{I}\cdot\mathbf{S} + (W_Sk_S + W_dd_e)\mathbf{S}\cdot\mathbf{n}\end{aligned} \quad . \qquad (1)$$

where **N** is the angular momentum operator excluding electronic spin, **S**, and nuclear spin, **I**, and **n** is a unit vector along the bond. The first five terms in Eq. 1 are commonly used to model the fine (via the *B* and γ terms), Fermi contact and dipolar magnetic hyperfine (via the b_F and *c* terms), and the electric quadrupole hyperfine (via the eq_0Q term) interactions. The sixth term describes the interaction of the anapole moment of the nucleus, k_A, with the electron spin, the seventh a scalar electron-nucleus interaction, and the last the interaction of d_e with the effective electric field, W_d. Determination of the

^{135}BaF and ^{137}BaF hyperfine parameters is particularly relevant to parity violation studies, because these parameters are the most sensitive probe of the electronic wavefunction in the region of the Ba nucleus. In parity non-conservation studies the constants W_A, W_S and W_d of Eq. 1 are calculated as expectation values of appropriate symmetry-violating operators over the electronic wavefunction in the region of the Ba nucleus. Thus, a comparison of experimentally measured hyperfine constants, which also depend upon the electronic wavefunction in the region of the Ba nucleus, is the most rigorous gauge of the reliability of the predicted W_A, W_S and W_d values.

Experimental schemes for measuring *P*- and *P*,*T*-odd effects in BaF exploit laser induced fluorescence detection using the $A\,^2\Pi - X\,^2\Sigma^+$ (0,0) band system. In addition, the study of *P*-odd effects relies on Zeeman tuning of opposite-parity levels to near degeneracy in a large magnetic field, and on mixing of these levels due to an applied electric field. Consequently, a spectroscopic understanding of the energy levels of both the $A\,^2\Pi(v = 0)$ and $X\,^2\Sigma^+$ ($v = 0$) states, as well as Stark and Zeeman effects in these states, is required. Here we report on the analysis of the $A\,^2\Pi - X\,^2\Sigma^+$ (0,0) band system recorded at near the natural linewidth limit (full width at half maximum (FWHM) ≈30 MHz). Spectra were recorded field-free and in the presence of static electric and magnetic fields. An improved set of fine and hyperfine parameters for the $A^2\Pi(\upsilon=0)$ state is determined for the ^{135}BaF, ^{137}BaF and ^{138}BaF isotopologues. The permanent electric dipole moment, μ_e, for the $A^2\Pi_{1/2}(\upsilon=0)$ and $A^2\Pi_{3/2}$ ($\upsilon=0$) states and the magnetic g-factors for the $A^2\Pi(\upsilon=0)$ and $X^2\Sigma^+(\upsilon=0)$ states of ^{138}BaF were determined from an analysis of the observed Stark and Zeeman shifts, respectively.

The field-free energies of the $X^2\Sigma^+(\upsilon=0)$ state of the ^{138}BaF and ^{137}BaF isotopologues are well characterized. The pure rotational spectra of ^{138}BaF [10] and ^{137}BaF [11] have been recorded and analyzed to produce a set of fine and hyperfine constants for the $X^2\Sigma^+(\upsilon=0)$ state. An improved set of ^{19}F magnetic hyperfine constant for the ^{138}BaF isotopologue was obtained from the analysis of the molecular beam laser-microwave double resonance spectrum [12]. In the same study, the electric field induced shifts of the rotational levels of the $X^2\Sigma^+(\upsilon=0)$ state were measured from which a μ_e of 3.170(3) D was determined. There have been no reported experimental measurement of μ_e for the $A^2\Pi$ state. The $X^2\Sigma^+(\upsilon=0)$ state has also been studied by high-resolution Fourier transform infrared emission spectroscopy [13]. In that study, numerous vibration-rotation bands were analyzed for the three most abundant isotopologues from which Dunham coefficients were derived.

The $A\,^2\Pi$ state is less well characterized. The $A\,^2\Pi - X\,^2\Sigma^+$ (0,0) band system of the main isotopologue, ^{138}BaF, has been previously characterized from analysis of the near Doppler limited resolution Fourier transform spectra of the thermal emission and the Ar^+ and Kr^+ ion laser induced fluorescence [14-16]. It was observed that the $A\,^2\Pi$ state was perturbed by the nearby $A'^2\Delta$ and $B\,^2\Sigma^+$ states. Effective molecular constants were obtained by treating the trio of states as a *d*-complex. The radiative lifetime of the $A\,^2\Pi_{1/2}(\upsilon=0)$ [17] and $A\,^2\Pi_{3/2}(\upsilon=0)$[18] states were measured to be 46.1 ns and 56.0 ns, respectively.

There are no high level *ab initio* predictions for the $X^2\Sigma^+$ and $A^2\Pi$ states. A semi-empirical electrostatic polarization model developed by Törring *et al* [19] predicts that μ_e

= 3.47D and 4.95D for the $X^2\Sigma^+$ and $A^2\Pi$ states, respectively. A similar model developed by Mestdagh and Visticot [20] predicts nearly identical values. A ligand field theory predictions [21] predicts μ_e = 3.89D and 3.45D for the $X^2\Sigma^+$ and $A^2\Pi$ states, respectively.

II. EXPERIMENT

The supersonic molecular beam production and laser induced fluorescent detection schemes are similar to those used in the previous measurements of SrF [22] and YbF [23,24]. A continuously rotating barium metal rod was ablated in a supersonic expansion of approximately 5% sulfur hexafluoride (SF_6) seeded in argon carrier gas with a backing pressure of approximately 3 MPa. The pulsed free-jet expansion was skimmed to form a well-collimated molecular beam which was crossed with a single longitudinal mode, continuous wave, Ti:Sapphire laser approximately 50 cm downstream from the source. The laser power was attenuated to approximately 20 mW and lightly focused (f.l.=1 m) to avoid power broadening. Spectral line widths of less than 40 MHz FWHM were observed.

The absolute wave numbers were determined to an accuracy of ± 0.003 cm^{-1} by simultaneously recording the Doppler limited I_2 absorption spectrum [25,26]. Interpolation between I_2 absorption features was achieved by simultaneously recording the transmission of two confocal étalons. One étalon was actively stabilized and calibrated to have a free spectral range of 749.14 MHz. A second, unstablized étalon with a free spectral range of 75.7 MHz was used to interpolate between transmission peaks of the stabilized étalon.

The optical Zeeman spectrometer [27] and optical Stark spectrometer [28] have been described previously. A 0 – 1.0 kG, homogeneous, magnetic field was generated using a homemade electromagnet in the interaction region of molecular beam and laser. The magnetic field was measure using a commercial Gauss meter. Static electric field strengths of up to 2000 V/cm were generated by application of a voltage across a pair of conducting plates straddling the region of molecular fluorescence. The electric field was measure by combination of a commercial volt meter and mechanical measurement of the plate separation. A polarization rotator and polarizing filter were used to orient the static electric or magnetic field vector of the linearly polarized laser radiation either parallel "||" or perpendicular "$_{\perp}$" to that of the applied field resulting in $\Delta M_F=0$ or $\Delta M_F=\pm 1$ selection rules. The combined systematic error associated with the measurement of the magnetic and electric field induced frequency shifts and the field strength is estimated to be less than 2%.

III. OBSERVATION

A. Field-free Spectra

Portions of the field-free excitation spectrum in the region of the $A^2\Pi_{1/2}$–$X^2\Sigma^+$ (0,0) and $A^2\Pi_{3/2}$–$X^2\Sigma^+$(0,0) sub-bands are presented in Figures 1 and 2, respectively. Enlarged portions of the field-free LIF spectra in the regions of the ${}^{R}R_{11}(4)$ (ν=11634.25 cm^{-1}) and ${}^{Q}Q_2(6)$ (ν=12260.60 cm^{-1}) lines are presented in Figures 3 and 4, respectively. The relative positions of the lines associated with the various isotopologues are evident in Figures 3 and 4. The spectra are congested in part because there are seven naturally occurring isotopes of barium: ^{130}Ba(0.11%), ^{132}Ba(0.10%), ^{134}Ba(2.42%), ^{135}Ba(6.59%),

^{136}Ba(7.85%), ^{137}Ba(11.23%) and ^{138}Ba(71.70%). Transitions associated with the ^{135}BaF, ^{136}BaF, ^{137}BaF and ^{138}BaF isotopologues are readily identified in Figures 1-3. Spectral lines of the odd isotopologues exhibit a large splitting due to a Ba-hyperfine interaction in the $X^2\Sigma^+(\upsilon=0)$ state. The nuclear magnetic g-factors for ^{135}Ba(**I**=3/2) and ^{137}Ba(**I**=3/2) are +0.5586 and +0.6249, respectively, and the quadrupole moments are +18 fm^2 and +28 fm^2, respectively. The ^{19}F(I=1/2) magnetic hyperfine splitting is much smaller because the unpaired electron in the $A^2\Pi$ and $X^2\Sigma^+$ states is centered on the metal nucleus. The predicted energy levels associated with lines of the ^{137}BaF isotopologue in the region of the $^{R}R_{11}(4)$ and $^{Q}Q_{2}(6)$ lines of the ^{138}BaF isotopologue, obtained using the finalized optimized parameters, are presented in Figures 5 and 6, respectively, and illustrates the relative hyperfine splitting.

The energy level patterns for the low-rotational levels of the $X^2\Sigma^+$ state of the even barium isotopologues are those of a molecule near the Hund's case ($b_{\beta J}$) limit with the approximately good intermediate quantum number J resulting from coupling the rotational angular momentum, **N**, with the electron spin angular momentum, **S.** Each rotational level of a given J of the even isotopologues splits into two levels designated by the total angular momentum F due to the ^{19}F(I=1/2) magnetic hyperfine splitting. The resulting Hund's case ($b_{\beta J}$) vector coupling appropriate for even barium isotopologues can be written as:

$$\mathbf{S} + \mathbf{N} = \mathbf{J};\ \mathbf{I_1}\ (^{19}\mathrm{F}) + \mathbf{J} = \mathbf{F}, \qquad (2)$$

which corresponds to the basis set $|\eta\Lambda\rangle|(SN)J(JI_1)F\rangle$.

The large ^{137,135}Ba magnetic hyperfine interaction in the $X^2\Sigma^+$ state causes the energy level pattern for the low-rotational levels of the odd isotopologues to be those of a molecule near the Hund's case ($b_{\beta S}$) limit. The approximately good intermediate quantum number G (=1 and 2) results from coupling the ^{137,135}Ba nuclear spin angular momentum, $\mathbf{I_1}$, with the total electron spin angular momentum, **S**. The ^{19}F nuclear spin is weakly coupled to **G** to produce the total angular momentum, **F**. The Hund's case ($b_{\beta S}$) vector coupling for low rotational levels can be written as:

$$\mathbf{S} + \mathbf{I_1}\,(^{137,135}\mathrm{Ba}) = \mathbf{G}\,(^{137,135}\mathrm{Ba});\ \mathbf{N} + \mathbf{G}(^{137,135}\mathrm{Ba}) = \mathbf{F}_1;\quad \mathbf{F}_1 + \mathbf{I}_2\,(^{19}\mathrm{F}) = \mathbf{F}, \tag{3}$$

which corresponds to the basis function $|\eta\Lambda\rangle|(SI_1)G(GN)F_1(F_1I_2)F\rangle$. The electron spin decouples from the nuclear spin with increasing rotation and the energy level pattern of the $X^2\Sigma^+$ state of odd isotopologues gradually transforms to that of a molecule near the Hund's case($b_{\beta J}$) limit. As an illustration, the energy level pattern of the $X^2\Sigma^+(v = 0)$ state of ^{137}BaF as a function of rotation, predicted using the previously determined fine and hyperfine parameters [11], is illustrated in Figure 7. The contribution due to rotation ($\approx B\times N(N+1)$) has been subtracted to emphasize the spin-rotation and hyperfine contributions.

The Ba hyperfine interactions are much smaller in the $A^2\Pi$ state and the energy level patterns for the low-rotational levels of both the even and odd barium isotopologues are those of a molecule near the Hund's case ($a_{\beta J}$) limit with the electron spin quantized

in the molecular frame and having a projection, Σ. A Hund's case ($a_{\beta J}$) coupling scheme, with the nuclear spin sequentially coupled, is appropriate for all the isotopologues;

$$\mathbf{J} + \mathbf{I}_1\,(^{135,137}\mathrm{Ba}) = \mathbf{F}_1; \quad \mathbf{F}_1 + \mathbf{I}_2\,(^{19}\mathrm{F}) = \mathbf{F}. \tag{4}$$

The corresponding basis function is $|\eta\Lambda\rangle|S\Sigma\rangle|J\Omega(JI_1)F_1(F_1I_2)F\rangle$. The inclusion of $\mathbf{I}_2$ (^{19}F), even though the ^{19}F(I=1/2) interaction is not fully resolved, facilitates spectral simulation.

A conventional $^2\Pi$ (*case* $a_{\beta J}$) - $^2\Sigma^+$ (*case* $b_{\beta J}$) labeling scheme of $^{\Delta N}\Delta J_{F_i'F_i''}(N'')$ [29], where F_i'' and F_i' subscripts designate the spin component of the $X^2\Sigma^+$ and $A^2\Pi$ states, respectively, is appropriate for the even isotopologues. In the cases where $\Delta N=\Delta J$ and $F_i'' = F_i'$ it is customary to drop the superscript and the second subscript. The twelve branches of the $^2\Pi$ (*case* $a_{\beta J}$) - $^2\Sigma^+$ (*case* $b_{\beta J}$) labeling scheme (P_1, Q_1, R_1, $^PQ_{12}$, $^OP_{12}$, $^QR_{12}$, P_2 , Q_2, R_2, $^RQ_{21}$, $^QP_{21}$, and $^SR_{21}$) are readily assigned (see Figures 1-4). The intermediate quantum number J is not appropriate for the low-rotational levels of the $X^2\Sigma^+$ state of the odd isotopologues and hence neither is the "F_i''" subscript in the conventional $^2\Pi$ (*case* $a_{\beta J}$) - $^2\Sigma^+$ (*case* $b_{\beta J}$) branch designation. It is customary to replace "F_i''" with the intermediate approximately good quantum number $G''$of the Hund's case ($b_{\beta S}$) coupling scheme. The twelve branches of the $^2\Pi$ (*case* $a_{\beta J}$) - $^2\Sigma^+$ (*case* $b_{\beta J}$) labeling scheme regroup into sixteen branch features of the $^2\Pi$ (*case* $a_{\beta J}$) - $^2\Sigma^+$ (*case* $b_{\beta S}$) scheme. The branches are designated as $^OP_{1G}$, $^PP_{1G} + {}^PQ_{1G}$, $^QQ_{1G} + {}^QR_{1G}$, and $^RR_{1G}$ for the $^2\Pi_{1/2}$

(*case* $a_{\beta J}$) - $^2\Sigma^+$ (*case* $b_{\beta S}$) sub-band and $^PP_{2G}$, $^QP_{2G} + {}^QQ_{2G}$, $^RQ_{2G} + {}^RR_{2G}$, and $^SR_{2G}$ for the $^2\Pi_{3/2}$ (*case* $a_{\beta J}$) - $^2\Sigma^+$ (*case* $b_{\beta S}$) sub-band with G= 1 and 2. The abbreviation $^PP_{1G}$, $^QQ_{1G}$, $^QP_{2G}$ and $^RQ_{2G}$ for the $^PP_{1G} + {}^PQ_{1G}$, $^QQ_{1G} + {}^QR_{1G}$, $^QP_{2G} + {}^QQ_{2G}$ and $^RQ_{2G} + {}^RR_{2G}$ branches, respectively, is used in Figures 3-6 and below.

A total of 439 transitions in the $A^2\Pi$-$X^2\Sigma^+$ (0,0) band were measured and assigned: 73, 99 and 267 for the ^{135}BaF, ^{137}BaF and ^{138}BaF isotopologues, respectively. The observed and calculated transition wave number, based upon the final optimized parameters, and associated assignments for the ^{138}BaF, ^{137}BaF, and^{135}BaF isotopologues are listed in Tables I, II and III, respectively, of the Supplemental Tables [30].

B. Stark Spectra

The $^SR_{21}(0)$ (ν=12262.88 cm^{-1}) and $^OP_{12}(2)$ (ν=11628.96 cm^{-1}) lines of the ^{138}BaF isotopologue were selected for optical Stark studies. The observed and predicted spectra for the $^SR_{21}(0)$ line recorded field-free and in the presence of a 899.4 V/cm static field with perpendicular orientation are presented in Figure 8. The associated energy levels as a function of applied field are also presented. The field free line rapidly splits into four components due to the near degeneracy of Λ-doublets associated with the J=3/2 level of the $A^2\Pi_{3/2}$ state. The pattern of four features slightly shifts to higher wave number due to the second order Stark tuning of the N=0 rotational level of the $X^2\Sigma^+$ state. The observed and predicted spectra for the $^OP_{12}(2)$ line recorded field-free and in the presence of a 2940 V/cm static field with parallel orientation are presented in Figure 9. The associated energy levels as a function of applied field are also presented. The field free spectral feature weakly tunes to lower wave number due primarily to the second order Stark

tuning in the *e*-parity component of the J=1/2 level of the $A^2\Pi_{1/2}$ state. The Λ-doubling of the J=1/2 level (i.e. the separation between the *e*- and *f*-parity components) is 0.2589 cm^{-1} (=p+2q). A total of 17 Stark induced shifts for the $^{S}R_{21}(0)$ line and 14 Stark induced shifts for the $^{O}P_{12}(2)$ line were assigned and precisely measured. Measured shifts and the difference between the measured and predicted shifts are listed in Table I.

C. Zeeman Spectra

The $R_1(0)$ (ν=11631.28 cm^{-1}) and $^{S}R_{21}(0)$ (ν=12262.88 cm^{-1}) lines of the ^{138}BaF isotopologue were selected for optical Zeeman studies. The $R_1(0)$ line recorded field free and in the presence of 714 G parallel and 724 G perpendicular magnetic fields are presented in Figure 10. The associated energy levels as a function of applied magnetic field, and the assignments, are also presented. The Zeeman tuning of the upper energy terminus of the $R_1(0)$ line (i.e. the "–" parity component of the J= 3/2 rotational level in the $A^2\Pi_{1/2}$ spin-orbit sub-state) is small and would be nearly zero in the Hund's case (*a*) limit. The $^{S}R_{21}(0)$ line recorded field-free and in the presence of a 192 G perpendicular magnetic field is presented in Figure 11. The associated energy levels as a function of applied magnetic field, and the assignments, are also presented. The Zeeman tuning of the upper energy terminus of the $^{S}R_{21}(0)$ line (i.e. "–" parity component of the J= 3/2 rotational level in the $A^2\Pi_{3/2}$ spin-orbit component) is significant because the energy level pattern is near Hund's case (*a*) limit. The measured thirty four magnetic induced shifts of the $^{S}R_{21}(0)$ line and forty two shifts of the $R_1(0)$ line, along with the quantum number assignments, are presented in Table II. The difference between the observed shifts and those predicted using the optimized magnetic g-factors (see below) is also given.

IV. ANALYSIS

A. Field Free

The observed transition wave numbers of the molecular beam optical spectrum were directly fit to an effective Hamiltonian for the $X^2\Sigma^+$ (v =0) and $A^2\Pi$ (v =0) state. The effective Hamiltonian for the $X^2\Sigma^+$ (v =0) state for the ^{138}BaF isotopologue was taken as:

$$\mathbf{H}^{\mathbf{eff}}(^2\Sigma^+) = B\mathbf{N}^2 - D\mathbf{N}^4 + \gamma\mathbf{N}\cdot\mathbf{S} + b_F(^{19}\mathrm{F})\mathbf{I}\cdot\mathbf{S} + c(^{19}\mathrm{F})\,(I_z S_z - \tfrac{1}{3}\mathbf{I}\cdot\mathbf{S}), \qquad (5)$$

where **N** is the angular momentum operator excluding electronic and nuclear spin, **S** and **I**, respectively. The effective Hamiltonian for the $X^2\Sigma^+$ (v =0) state for the ^{135}BaF and ^{137}BaF isotopologues were taken as that of Eq. 5 with the addition of Fermi contact, dipolar and electric quadrupole terms for ^{135}Ba and ^{137}Ba :

$$b_F(^{135,137}\mathrm{Ba})\mathbf{I}\cdot\mathbf{S} + c(^{135,137}\mathrm{Ba})\,(I_z S_z - \tfrac{1}{3}\mathbf{I}\cdot\mathbf{S}) + eq_0 Q(^{135,137}\mathrm{Ba})\frac{3I_z - \mathbf{I}^2}{4I(2I-1)} \quad . \qquad (6)$$

The field-free eigenvalues and eigenvectors for the $X^2\Sigma^+$ (v =0) state were obtained by numerical diagonalization of the representation constructed in a sequentially coupled Hund's case ($a_{\beta J}$) basis set. The representation for ^{138}BaF was of dimension 4 (= $(2S+1)\times(2I(^{19}\mathrm{F})+1)$) whereas the representation for the odd isotopologues was 16 (= $(2S+1)\times(2I(^{19}\mathrm{F})+1)\times(2I(^{135,137}\mathrm{Ba})+1)$. The expressions for the matrix elements were taken from Ref. 31.

Combination difference revealed that the $A^2\Pi_{3/2}$ (v=0) sub-state levels of the ^{135}BaF and ^{137}BaF isotopologues exhibited no magnetic hyperfine splitting. Furthermore, no Λ-doubling in the $A^2\Pi_{3/2}$ (v =0) sub-state was observed. The Λ-doubling in Hund's case (a) limit $^2\Pi_{3/2}$ and $^2\Pi_{1/2}$ sub-state goes approximately as qJ^2 and $(p+2q)J$ [31], respectively. Therefore, the energies for the $A^2\Pi$ (v =0) state were modeled by including the origin ($T_{0,0}$), spin-orbit interaction (A) and the associated centrifugal distortion correction (A_D), rotation (B) and associated centrifugal distortion correction (D), the Λ-doubling (p+2q) (which affects the $A^2\Pi_{1/2}$ (v =0) sub-band), and the Λ-type magnetic hyperfine d(^{135,137}Ba) interaction terms :

$$\mathbf{H^{eff}}(^2\Pi) = T_{0,0} + AL_zS_z + \tfrac{1}{2}A_D[L_zS_z,\mathbf{R}]^+ + B\mathbf{R^2} - D(\mathbf{R^2})^2 + \tfrac{1}{2}(p+2q)(e^{-2i\phi}J_+S_+ + e^{+2i\phi}J_-S_-) + \tfrac{1}{2}d(e^{-2i\phi}I_+S_+ + e^{+2i\phi}I_-S_-). \quad (7)$$

In Eq. 7 $J_\pm$, $S_\pm$ and $I_\pm$ are the shift operators of the total angular momentum in the absence of nuclear spin, **J,** the total electron spin, **S**, and the ^{135,137}Ba nuclear spin angular momentum, $\mathbf{I_1}$, and ϕ is the azimuthal coordinate of the electrons. $[L_zS_z,\mathbf{R}]^+$ is the anti-commutator. The field-free eigenvalues and eigenvectors for the $A^2\Pi$ (v =0) state were obtained by numerical diagonalization of the representation constructed in a sequentially coupled Hund's case ($a_{\beta J}$) basis set. The representation for ^{138}BaF was of dimension 8 (= 2×(2S+1)×(2I(^{19}F)+1)) whereas the representation for the odd isotopologues was 32(=2×(2S+1)×(2I(^{19}F)+1)×(2I(^{135,137}Ba)+1). The expressions for the matrix elements were taken from Ref. 31.

Various fits of the measured field-free spectrum were performed. The 267 measured field-free transitions [30] for the ^{138}BaF isotopologue were modeled by varying

$T_{0,0}$, A, A_D, B and $(p+2q)$. The centrifugal distortion correction to the rotational parameters, D, for the $A^2\Pi$ (v =0) state was held fixed to the value determined from the analysis of the high temperature optical spectrum [15]. For the $X^2\Sigma^+$ (v =0) state, the B and γ parameters were constrained to the microwave values [10], the magnetic hyperfine parameters $b_F(^{19}\text{F})$ and $c(^{19}\text{F})$ were constrained to MODR values [12] and D to the high temperature optical spectrum [15]. The optimized parameters and associated errors are given in Table III. The standard deviation of the fit (=0.0013 cm^{-1}) is commensurate with the estimated measurement error.

Least squares fitting of the 99 measured lines for the ^{137}BaF isotopologue [30] proceeded in a similar fashion. The fine and magnetic hyperfine parameters of the $X^2\Sigma^+$ (v =0) state were constrained to values extracted from the analysis of the pure rotational spectrum [11] with the exception of D which was constrained to the value obtained from the analysis of ^{138}BaF optical spectrum [15] scaled by the expected mass ratio (i.e. scaled by $[\mu(^{138}\text{BaF})]^2/[\mu(^{137}\text{BaF})]^2$ where μ=reduced mass). Five parameters for the $A^2\Pi$ (v =0) state were varied: A, B, $(p+2q)$, $d(^{137}\text{Ba})$ and T_{00}. A_D was constrained to the value extracted from the analysis of the ^{138}BaF measurements [11] and D to the value obtained from isotopically scaling the ^{138}BaF value. The optimized parameters and associated errors are given in Table III. The standard deviation of the fit (=0.0014 cm^{-1}) is commensurate with the estimated measurement error.

There are no previously determined parameters for the ^{135}BaF isotopologue. Fitting of the 73 measured and assigned transitions [30] was performed by varying a subset of both the $X^2\Sigma^+$ (v =0) and $A^2\Pi$ (v =0) state parameters. In the $X^2\Sigma^+$ (v =0) state only B and b_F (Ba) were varied. The parameter D was constrained to the ^{138}BaF scaled by

the known mass dependence and the $c(^{135}\mathrm{Ba})$ and eQq_0 (^{135}Ba) parameters to those for ^{137}Ba scaled by the nuclear g-factors and quadrupole moment, respectively. The fluorine magnetic hyperfine parameters for ^{137}BaF, $b_F(^{19}\mathrm{F})$ and $c(^{19}\mathrm{F})$, were constrained to the ^{138}BaF values [10]. The origin, T_{00}, rotational constant, B, and spin-orbit parameter, A, for the $A^2\Pi$ (v =0) state of the ^{137}BaF isotopologue were varied. The parameters A_D and ($p+2q$) were constrained to the ^{138}BaF values, D to the mass scaled ^{138}BaF value and d(Ba) to the ^{137}BaF value scaled by the nuclear g-factors. The standard deviation of the fit (=0.0015 cm^{-1}) is commensurate with the estimated measurement error.

B. Stark Effect and Intensities

The interaction between the static electric field, **E**, and the molecular electric dipole moment operator, $\boldsymbol{\mu}$, is represented by the Stark Hamiltonian,

$$\mathbf{H}^{\mathrm{Stark}} = -\boldsymbol{\mu}\cdot\mathbf{E}. \tag{8}$$

The matrix representation of $\mathbf{H}^{\mathrm{Stark}}$ is block diagonal in M_F but of infinite dimension. The predicted Stark shifts in the $X^2\Sigma^+(v=0)$ state of the ^{138}BaF isotopologue were obtained by numerical diagonalization of a 16×16 truncated matrix representation constructed using the Hund's case ($a_{\beta J}$) basis functions for F=0-4. The observed Stark shifts of Table I were used as input into a non-linear least-squares fitting program in which μ_e for the $X^2\Sigma^+(v=0)$ was held fixed to the previously determined value (=3.170(3)D) [12] and μ_e for the $A^2\Pi$ (v =0) state was optimized. Initial attempts to simultaneously fit the shifts of the $^{S}R_{21}(0)$ and $^{O}P_{12}(2)$ lines revealed systematic deviations indicating that the μ_e values for the $A^2\Pi_{1/2}$ and $A^2\Pi_{3/2}$ spin-orbit states are

significantly different. Independent fits of the Stark shifts of the ${}^{S}R_{21}(0)$ and ${}^{O}P_{12}(2)$ lines determined μ_e of 1.50(2) D and 1.31(2) D for the $A^2\Pi_{1/2}(\upsilon=0)$ and $A^2\Pi_{3/2}$ ($\upsilon=0$) states, respectively. The error estimates represent a 90% confidence limit. The standard deviation of the fits for the ${}^{S}R_{21}(0)$ and ${}^{O}P_{12}(2)$ lines were 8 MHz and 5 MHz, respectively, which are commensurate with the measurement uncertainty.

Modeling the spectra greatly assisted in the assignment of quantum numbers, particularly in the case of the overlapped spectra for the ^{135}BaF and ^{137}BaF isotopologues. Spectra for the ^{138}BaF isotopologue were modeled by constructing a 4×8 Hund's case ($a_{\beta J}$) electric dipole transition moment matrix and cross multiplying the transition matrix by the $X^2\Sigma^+$ and $A^2\Pi$ (v=0) eigenvectors. The transition moment was squared, multiplied by a Boltzmann factor and a Lorentzian line shape was superimposed on each spectral feature and co-added. Spectra for the ^{135}BaF and ^{137}BaF isotopologues were modlled in a similar fashion, but with 16×32 Hund's case ($a_{\beta J}$) electric dipole transition moment matrix.

C. Zeeman Effect

The effective Zeeman Hamiltonian was taken as [31, 32]:

$$\begin{aligned}\hat{\mathbf{H}}^{Zee}(eff) &= g_S\mu_B\hat{\mathbf{S}}\cdot\hat{\mathbf{B}} + g_L'\mu_B\hat{\mathbf{L}}\cdot\hat{\mathbf{B}} + \\ &g_{\parallel}\mu_B(\hat{S}_x\hat{B}_x + \hat{S}_y\hat{B}_y) + g_{\parallel}'\mu_B(e^{-2i\phi}\hat{S}_+\hat{B}_+ + e^{+2i\phi}\hat{S}_-\hat{B}_-)\cdot\end{aligned} \tag{9}$$

The rotational g-factors, g_r and g_r', were not included because their effects are expected to be negligibly small for the low-rotational levels investigated. In the effective Hamiltonian model, both g_S and g_L' are treated as adjustable parameters to account for electronic state mixing [31].

The matrix representation of $\hat{\mathbf{H}}^{Zee}(eff)$ is of infinite order. The very small ^{19}F magnetic hyperfine splitting was not resolved in the Zeeman spectra (see Figures 10 and 11) due to inhomogeneous and residual fields and the energy levels can be characterized by the projection quantum number M_J. Eigenvalues and eigenvectors for the lowest rotational levels of the $A^2\Pi(v=0)$ and $X^2\Sigma^+(v=0)$ states investigated here were obtained by numerical diagonalization of an 8×8 and 16×16 matrix representations, respectively, constructed from the J=0.5 to J=3.5 Hund's case (a) basis functions. The expressions for the matrix elements were taken from Ref. 31. The 76 magnetically-induced Zeeman shifts of Table II, and initial estimates of the g-factors for the $A\ ^2\Pi(v=0)$ and $X\ ^2\Sigma^+$ (v=0) states, were input for a nonlinear least square fitting process. Initial attempts to simultaneously optimize g_S, g'_L, g_l and g'_l for the $A^2\Pi$ state and g_l and g_S for $X\ ^2\Sigma^+$ produced a highly correlated set of parameters. In the end, the g_S parameter for the $A^2\Pi$ (v=0) and $X\ ^2\Sigma^+$ (v=0) states was held fixed at 2.002 because the non-adiabatic contributions to this parameter are expected to be small [31]. In addition, $g_l(A^2\Pi)$, which is predicted to be small (*vide infra*) was set to zero. The optimized values for g_l ($X^2\Sigma^+(v=0)$), g'_l ($A^2\Pi(v=0)$) and g'_L ($A^2\Pi(v=0)$) along with their associated errors and correlation matrix, are listed in Table V. The standard deviation of the fit was 34 MHz, which is commensurate with the estimated measurement accuracy.

V. DISCUSSION

A primary objective of the current study was to determine a set of spectroscopic parameters that can be used to predict the eigenvalues and eigenvectors for the $A^2\Pi(v=0)$

and $X\,^2\Sigma^+$ (v=0) states of the three major isotopologues of barium monofluorides, both field-free and in the presence of static magnetic and electric fields. As can be seen from the comparison of the predicted and observed spectra given in Figures 3-6, 8 and 9 the determined spectroscopic constants accurately reproduce the energies and eigenvectors at fields appropriate for future PNC measurements. The observed ^{135}Ba and ^{137}Ba hyperfine structure in the low-rotational levels of the $A^2\Pi_{1/2}(v=0)$ sub-state can be modeled using solely the d(Ba) magnetic hyperfine parameter. The $A^2\Pi_{3/2}(v=0)$ sub-state exhibited no hyperfine structure.

Surprisingly, the semi-empirical electrostatic model predictions by Törring *et al* [19] and Mestdagh and Visticot [20] which predict μ_e values of approximately 5D for the $A^2\Pi$ which are in very poor agreement with observation. The LFT prediction [21] of 3.45D for the $A^2\Pi$ states is only slightly better. The determined μ_e values for BaF are compared with values for isovalent CaF [33,34] and SrF [35, 36] in Table V. Only the μ_e values for the $A^2\Pi_{3/2}$ (υ=0) spin-orbit state were measured for CaF and SrF. For all three molecules there is an observed large decrease in μ_e upon excitation from the $X\,^2\Sigma^+$ state to the $A^2\Pi$ state. This is qualitatively explained as the result of promoting the sole unpaired electron from a metal ion-centered n*s* orbital (n=*4,5,* and 6 for Ca, Sr and Ba) to a more highly polarizable $np_{\pm 1}/(n-1)d_{\pm 1}$ hybrid orbital. The effect becomes more pronounced down the series with the ratios $\mu_e\,(A^2\Pi_{3/2})/\mu_e\,(X\,^2\Sigma^+)$ being 0.79, 0.59 and 0.41 for CaF, SrF and BaF, respectively. This mimics the trend in static average electric dipole polarizabilities for the ground states of Ca (=23 Å^3), Sr(=28 Å^3) and Ba (=56 Å^3).

The observation that μ_e ($A^2\Pi_{1/2}$) (=1.50(2) D) is larger than μ_e ($A^2\Pi_{3/2}$) (=1.31(2) D) must result from a complicated spin-orbit mixing of the $A^2\Pi$ state with the nearby $A'^2\Delta$ ($T_e\approx$ 10940 cm^{-1}), $B^2\Sigma^+$ ($T_e\approx$ 14040 cm^{-1}) and $C^2\Pi$ ($T_e\approx$ 20091 cm^{-1}) states. LFT [20], which does not account for spin-orbit mixing, predicts that $\mu_e(A'^2\Delta)$ and μ_e ($C^2\Pi$) are greater than $\mu_e(A^2\Pi)$ which in turn is comparable to $\mu_e(B^2\Sigma^+)$. According to LFT, μ_e ($A'^2\Delta$) is large because, to a first approximation, the sole unpaired electron is in a compact Ba^+-centered 5*d* orbital and $\mu_e(C^2\Pi)$ is large because the sole unpaired electron is in a Ba^+-centered 5*d*-6*p* hybrid orbital that is pointed towards the F-nucleus. Furthermore, according to LFT $\mu_e(A^2\Pi)\approx\mu_e(B^2\Sigma^+)$ because the LFT predicted 5*d* and 6*p* composition for the two states is approximately identical. Evidently the $A^2\Pi_{1/2}$ state is more strongly mixed with the $C^2\Pi$ and $A'^2\Delta$ states than is the $A^2\Pi_{3/2}$ state. A similar effect has been observed in CaOH and SrOH [36].

The determined Zeeman parameters can also be qualitatively understood. An estimate for g_l ($X^2\Sigma^+$) is obtainable from the Curl relationship [32]:

$$g_l \approx -\gamma / 2B, \qquad (8)$$

where γ and B, are the spin-rotation and rotational parameters. Using the parameters from Table III, Eq. 8 gives g_l($X^2\Sigma^+$) = -0.00625 which is the correct sign but about a factor of four too small. The parity-dependent anisotropic *g*-factor for the $A^2\Pi$ state can be approximated using an equation analogous to the Curl relationship [31]:

$$g_l' \approx p / 2B, \qquad (9)$$

where p is the Λ-doubling parameter. It is reasonable to assume that q=0, and thus that p=-0.2575 cm^{-1}, since no Λ-doubling in the $A^2\Pi_{3/2}$ levels was observed. Eq. 9 predicts that $g_l' \approx$ -0.2575/(2×0.21954) = -0.5866 , which is in very good agreement with the experimental value (= -0.536(23)). In fitting the Zeeman shifts, g_l for the $A^2\Pi$ was constrained to zero. It is difficult to estimate g_l for the $A^2\Pi$ from the Curl relationship (Eq. 8) because the required spin-rotation parameter, γ, for the $A\ ^2\Pi$ state is not determined. Brown and Watson [36] have shown that for a $^2\Pi$ state γ and A_D, the centrifugal distortion correction to the spin-orbit coupling, are totally correlated. When γ is constrained to zero, as was done here, then the fitting parameter A_D is a linear combination of the true values for A_D and γ [37]:

$$A_D^{Fitting} \approx A_D^{True} - \gamma \frac{2B}{(A-2B)} \quad . \qquad (10)$$

An upper limit for γ ($A\ ^2\Pi$) of -0.046 cm^{-1} is obtained from Eq. 10 by assuming that A_D^{True} = 0. The Curl relationship then predicts that an approximate value for g_l ($A\ ^2\Pi$) of +0.11.

VI. CONCLUSION

A cold molecular beam sample of BaF has been generated by laser vaporization techniques and the $A^2\Pi$-$X^2\Sigma^+$ (0,0) band system recorded at near the natural linewidth limit both field-free and in the presence of static magnetic and electric fields. A set of effective spectroscopic parameters has been generated that can reproduce the energies at

field strengths appropriate for proposed PNC measurements. The determined hyperfine parameters, magnetic g-factors and permanent electric dipole moments are benchmarks for evaluation of future predictions of the excited $A^2\Pi$ state.

Acknowledgements.

This research has been supported by the National Science Foundation –Experimental Physical Chemistry (Grant 943360412) and Physics (Grant PHY-0758045). The authors would like to thank Dr. Jinhai Chen for assistance in the measurements.

Figure Captions

Figure 1. The field-free spectrum of $A^2\Pi_{1/2}$-$X^2\Sigma^+$(0,0) sub-band system of BaF.

Figure 2. The field-free spectrum of $A^2\Pi_{3/2}$-$X^2\Sigma^+$(0,0) sub-band system of BaF.

Figure 3. The observed and predicted spectra of the $A^2\Pi_{1/2}$-$X^2\Sigma^+$(0,0) sub-band system of BaF in the region of the $R_1(4)$ line (ν=11634.25 cm^{-1}) of the ^{138}BaF isotopologue. The predicted spectra were obtained using the optimized parameters of Table III and a linewidth of 20 MHz.

Figure 4. The observed and predicted spectra of the $A^2\Pi_{3/2}$-$X^2\Sigma^+$(0,0) sub-band system of BaF in the region of the $Q_2(6)$ line (ν=12260.60 cm^{-1}) and $^{Q}P_{21}(6)$ line (ν=12260.58 cm^{-1}) of the ^{138}BaF isotopologue. The predicted spectra were obtained using the optimized parameters of Table III and a linewidth of 20 MHz.

Figure 5. The predicted energy level pattern associated with the $^{R}R_{12}(4)$ line (ν=11634.19 cm^{-1}) and the $^{R}R_{11}(4)$ line (ν=11634.35 cm^{-1}) line of the ^{137}BaF isotopologue. The assignment of the spectral features of Figure 3 are indicated. The energies were calculated using the optimized parameters of Table III.

Figure 6. The predicted energy level pattern associated with the $^{Q}P_{22}(6)$ line (ν=12260.52 cm^{-1}) and the $^{Q}P_{21}(6)$ line (ν=12260.68 cm^{-1}) line of the ^{137}BaF

isotopologue. The assignment of the spectral features of Figure 4 are indicated. The energies were calculated using the optimized parameters of Table III.

Figure 7. The ^{137}BaF isotopologue spin-rotation and hyperfine energy level pattern for the $X\,^2\Sigma^+$ (v =0) state as a function of rotational quantum number, N. The low-rotational levels are those of a Hund's case($b_{\beta S}$) molecule with G being the appropriate intermediate quantum number and those of the high rotational levels a Hund's case($b_{\beta J}$) molecule where J is the appropriate intermediate quantum number.

Figure 8. The observed and predicted $^{S}R_{21}(0)$ line of the ^{138}BaF isotopologue recorded field-free and in the presence of a 899.4 V/cm static field with perpendicular orientation and the associated energy levels as a function of applied field. The near degeneracy of the Λ-doublets in the J=3/2 level of the $A^2\Pi_{3/2}$ state results in a linear Stark tuning of the energy levels.

Figure 9. The observed and predicted $^{O}P_{12}(2)$ line of the ^{138}BaF isotopologue recorded field-free and in the presence of a 2940.9 V/cm static field with parallel orientation and the associated energy levels as a function of applied field. The large Λ-doubling (=0.257 cm^{-1}) of the J=1/2 levels of the $A^2\Pi_{1/2}$ state results in a second order Stark effect.

Figure 10. The $R_1(0)$ line of the ^{138}BaF isotopologue recorded field free (bottom) and in the presence of 713 G parallel (middle) and a 724 G perpendicular (top) magnetic fields.

The associated energy levels as a function of applied magnetic field, and the assigned transitions, are also presented.

Figure 11. The ${}^{S}R_{21}(0)$ line of the ^{138}BaF isotopologue recorded field-free (bottom) and in the presence of a 192 G perpendicular (top) magnetic field. The associated energy levels as a function of applied magnetic field, and the assigned transitions, are also presented.

Reference

1. M. G.Kozlov, A. V.Titov, N. S.Mosyagin, and P. V. Souchko, Phys. Rev. A: Atomic, Molecular, and Optical Physics **56**, R3326 (1997).
2. A. V.Titov, N. S.Mosyagin, A. N. Petrov, and T. A. Isaev, Int. J. of Quantum Chemistry **104**, 223 (2005).
3. M. K. Nayak, and R. K. Chaudhuri, J. Phys. B: Atomic, Molecular and Optical Physics **39**, 1231 (2006).
4. A. V.Titov, N. S.Mosyagin, A. N. Petrov, T. A. Isaev, and D. P. DeMille, Progress in Theoretical Chemistry and Physics, **15** (Recent Advances in the Theory of Chemical and Physical Systems), 253 (2006).
5. M. K.Nayak, R.K.Chaudhuri, and B. P. Das, Phys. Rev. A: Atomic, Molecular, and Optical Physics **75**, 022510 (2007).
6. M. K. Nayak and R. K.Chaudhuri, Phys. Rev. A: Atomic, Molecular, and Optical Physics **78**, 012506 (2008).
7. M. K.Nayak and B. P. Das, Phys. Rev. A: Atomic, Molecular, and Optical Physics **79**, 060502 (2009).
8. D. DeMille, S. B. Cahn, D. Murphree, D. A. Rahmlow, and M. G. Kozlov, Phys. Rev. Lett. **100**, 023003(2008)
9. M. G. Kozlov and L. N. Labzowsky, J. Physics B: Atomic, Molecular and Optical Physics **28**, 1933 (1995).
10. Ch. Rayzlewicz and T. Törring, Chem. Phys. **51**, 329 (1980).

11. Ch. Rayzlewicz, H.-U. Schütze-Pahlmann, J. Hoeft and T. Törring, Chem. Phys. **71**, 389 (1982).

12. W.E. Ernst, J. Kändler, and T. Törring, J. Chem. Phys. **84**, 4769 (1986).

13. B. Guo, K. Q. Zhang, and P.F. Bernath, J. Mol. Spectrosc. **170**, 59, (1995).

14. C. Effantin, A. Bernard, J. D'Incan, G. Wannous, J. Verges, and R. F. Barrow, Mol. Physics **70**, 735 (1990).

15. A. Bernard, C. Effantin, J. D'Incan, J. Verges, and R. F. Barrow, Mol. Physics **70**, 747 (1990).

16. A. Bernard, C. Effantin, E. Andrianavalona, J. Verges, and R. F. Barrow, J. Mol. Spectrosc. **152**, 174 (1992).

17. L.-E. Berg, N. Gador, D. Husain, H. Ludwigs, and P. Royen, Chem. Phys. Lett. **287**, 89 (1998).

18. L.-E.Berg, T. Olsson, J. C. Chanteloup, A. Hishikawa, and P. Royen, Mol. Phys. **79**, 721 (1993).

19. T. Törring, W.E. Ernst, and J. Kändler, J. Chem. Phys. **90**, 4927 (1989).

20. J.M. Mestdagh and J.P. Visticot, Chem. Phys. **155**, 79 (1991).

21. A. R. Allouche, G. Wannous and M. Aubert-Frécon, Chem. Phys. **170**, 11 (1993).

22. A.T. Le, H. Wang, and T.C. Steimle, Phys. Rev. **80**, 062513 (2009).

23. T.C. Steimle, T. Ma and C. Linton, J. Chem. Phys. **127**, 234316 (2007).

24. T. Ma, C. Butler, J.M. Brown, C. Linton and T.C. Steimle, J. Phys. Chem. A. **113**, 8038 (2009).

25. S. Gerstenkorn and P. Luc, *Atlas du spectre d'absorption de la mol☺cule de l'iode*(Editions du C.N.R.S.) (1978); Rev. Phys. Appl. **14**, 791 (1979).

26. S. Gerstenkorn, P. Luc and R. Vetter, Rev. Phys. Appl. **16** 529 (1981).

27. T. C. Steimle, J. Gengler, and J. Chen, Can. J. Chem. **82**, 779 (2004).

28. T. C. Steimle, Int. Rev. Phy. Chem. **19,** 455 (2000).

29. G. Herzberg, *Molecular Spectra and Molecular Structure* (Van Nostrand Reinhold Company, New York, 1950).

30. See EPAPS Document No. [*number will be inserted by publisher*] for supplemental tables. This document can be reached via a direct link in the online article's HTML reference section or via the EPAPS homepage http://0-www.aip.org.library.lib.asu.edu/pubservs/epaps.html.

31. J. M. Brown and A. Carrington, *Rotational Spectroscopy of Diatomic Molecules* (Cambridge University Press, Cambridge, 2003).

32. W.Weltner, Jr., 1983, *Magnetic Atoms and Molecules,* (New York, Dover Publications Inc.)

33. W. J. Childs, L. S. Goodman, U. Nielsen, and V. J. Pfeufer, Chem. Phys. **80**, 2283 (1984).

34. W. E. Ernst and J. Kaendler, Phys. Rev. A: Atomic, Molecular, and Optical Physics **39**, 1575 (1989).

35. W. E. Ernst, J. Kaendler, S.Kindt, and T. Toerring, Chem. Phys. Lett. **113**, 351 (1985).

36. J. Kaendler, T. Martell, and W. E. Ernst, Chem. Phys. Lett. **155**, 470 (1989).

37. T.C. Steimle, D.A. Fletcher, K.Y. Jung and C.T. Scurlock, J. Chem. Phys. **96**, 2556 (1992).

38. J. M. Brown and J .K. G. Watson J. Mol. Spectrosc. **65**, 65 (1977).

Supplemental Table I. The observed and calculated transition wave numbers (cm^{-1}) for the $A^2\Pi$-$X^2\Sigma^+$ (0,0) band system of ^{138}BaF.

Branch	N''	Observed	Obs.-Cal.	Branch	N''	Observed	Obs.-Cal.
P_1	1	11630.0816	-0.0010	Q_1	12	11630.5669	0.0012
	2	11629.9810	-0.0002		13	11630.5366	0.0013
	3	11629.8720	0.0008		14	11630.4971	0.0009
	4	11629.7541	0.0015		15	11630.4504	0.0020
	5	11629.6262	0.0007		16	11630.3924	0.0004
	6	11629.4892	-0.0005		17	11630.3279	0.0010
	7	11629.3446	-0.0008		18	11630.2548	0.0016
	8	11629.1931	0.0005		19	11630.1700	-0.0007
	9	11629.0316	0.0005		20	11630.0816	0.0020
	10	11628.8612	0.0002		21	11629.9810	0.0013
	11	11628.6827	0.0003		22	11629.8720	0.0009
	12	11628.4951	-0.0001		23	11629.7541	0.0003
	13	11628.2977	-0.0017		24	11629.6284	0.0007
	14	11628.0966	0.0016		25	11629.4933	0.0004
	15	11627.8832	0.0012		26	11629.3497	0.0003
$^OP_{12}$	2	11628.9683	0.0007		27	11629.1980	0.0010
	3	11628.1797	0.0002		28	11629.0366	0.0007
	4	11627.3818	-0.0010		29	11628.8665	0.0006
	10	11622.4214	-0.0015		30	11628.6872	0.0000
P_2	3	12260.2951	-0.0008		31	11628.4990	-0.0006
	4	12259.6279	-0.0010		32	11628.3024	-0.0008
	5	12258.9527	-0.0009		33	11628.0966	-0.0014
	6	12258.2681	-0.0020		34	11627.8832	-0.0006
$^QP_{21}$	2	12261.5823	-0.0002	$^PQ_{12}$	1	11630.0869	-0.0007
	3	12261.3437	-0.0009		2	11629.9883	-0.0006
	4	12261.0967	-0.0018		3	11629.8808	-0.0009
	5	12260.8446	0.0005		4	11629.7648	-0.0010
	6	12260.5807	-0.0008		5	11629.6406	-0.0008
	7	12260.3100	-0.0007		6	11629.5071	-0.0012
	8	12260.0327	0.0010		7	11629.3657	-0.0010
	9	12259.7444	0.0000		8	11629.2161	-0.0005
	10	12259.4489	0.0000		9	11629.0577	-0.0001
	11	12259.1439	-0.0012		10	11628.8898	-0.0006
	12	12258.8337	0.0006		11	11628.7136	-0.0009
	13	12258.5126	-0.0003		12	11628.5298	-0.0002
	14	12258.1842	-0.0002		13	11628.3389	0.0020
	15	12257.8477	0.0000		14	11628.1358	0.0006
Q_1	0	11630.2581	-0.0001		15	11627.9250	0.0001
	0	11630.2601	-0.0003	Q_2	2	12261.5890	-0.0013
	1	11630.3321	0.0009		3	12261.3531	-0.0020
	2	11630.3956	0.0001		4	12261.1093	-0.0024
	3	11630.4518	0.0005		5	12260.8592	-0.0008
	4	11630.4971	-0.0014		6	12260.5986	-0.0015
	5	11630.5366	-0.0004		7	12260.3299	-0.0021
	6	11630.5669	-0.0001		8	12260.0550	-0.0007
	7	11630.5880	-0.0003		9	12259.7702	-0.0009
	8	11630.6004	-0.0006		10	12259.4770	-0.0013

	9	11630.6055	0.0004		11	12259.1754	-0.0018
	10	11630.6023	0.0017		12	12258.8675	-0.0004
	11	11630.5880	0.0005		13	12258.5492	-0.0012

Supplemental Table 1 (Continued)

Branch	N''	Observed	Obs.-Cal.	Branch	N''	Observed	Obs.-Cal.
Q_2	14	12258.2236	-0.0010	${}^{R}Q_{21}$	52	12261.6583	0.0004
	15	12257.8892	-0.0014		53	12261.4192	0.0003
${}^{R}Q_{21}$	1	12262.4466	-0.0010		54	12261.1694	-0.0016
	2	12262.6408	-0.0008		55	12260.9135	-0.0007
	3	12262.8273	-0.0001		56	12260.6476	-0.0009
	4	12263.0046	-0.0003		57	12260.3719	-0.0018
	5	12263.1729	-0.0012		58	12260.0868	-0.0032
	6	12263.3338	-0.0013		59	12259.7952	-0.0021
	7	12263.4874	-0.0004	R_1	0	11631.2805	0.0010
	8	12263.6320	-0.0003		0	11631.2825	0.0008
	9	12263.7687	0.0002		1	11632.0350	0.0016
	10	12263.8973	0.0009		2	11632.7792	0.0006
	11	12264.0152	-0.0008		4	11634.2447	0.0016
	12	12264.1239	-0.0034	${}^{Q}R_{12}$	1	11630.3339	-0.0023
	13	12264.2297	-0.0006		2	11630.4028	-0.0005
	14	12264.3270	0.0020		3	11630.4609	-0.0009
	15	12264.4119	0.0005		4	11630.5118	0.0001
	16	12264.4894	-0.0001		5	11630.5525	-0.0004
	17	12264.5597	0.0005		6	11630.5851	-0.0005
	18	12264.6216	0.0010		7	11630.6055	-0.0041
	19	12264.6732	-0.0004		8	11630.6244	-0.0006
	20	12264.7190	0.0007		9	11630.6315	-0.0003
	21	12264.7560	0.0013		10	11630.6299	-0.0001
	22	12264.7845	0.0019		11	11630.6196	0.0000
	23	12264.8041	0.0020		12	11630.5976	-0.0029
	24	12264.8140	0.0007		13	11630.5724	-0.0004
	25	12264.8166	0.0006		14	11630.5366	0.0002
	26	12264.8118	0.0015		15	11630.4908	-0.0005
	27	12264.7982	0.0020		16	11630.4369	-0.0007
	28	12264.7751	0.0015		17	11630.3755	0.0003
	29	12264.7438	0.0012		18	11630.3039	-0.0003
	30	12264.7046	0.0015		19	11630.2249	0.0005
	31	12264.6575	0.0024		20	11630.1381	0.0021
	32	12264.6007	0.0021		21	11630.0397	0.0009
	33	12264.5350	0.0015		22	11629.9335	0.0006
	34	12264.4613	0.0013		23	11629.8188	0.0005
	35	12264.3797	0.0018		24	11629.6948	-0.0001
	36	12264.2896	0.0024		25	11629.5618	-0.0010
	37	12264.1893	0.0013		26	11629.4209	-0.0010
	38	12264.0830	0.0029		27	11629.2723	0.0000
	39	12263.9647	0.0010		28	11629.1141	0.0002
	40	12263.8421	0.0035		29	11628.9463	-0.0003
	41	12263.7071	0.0022		30	11628.7705	-0.0001
	42	12263.5648	0.0023		31	11628.5847	-0.0010
	43	12263.4126	0.0012		32	11628.3909	-0.0011

	44	12263.2522	0.0006		33	11628.1894	0.0000
	45	12263.0831	0.0000		34	11627.9776	-0.0004
	46	12262.9079	0.0020	R_2	1	12262.4509	-0.0018
	47	12262.7209	0.0010		2	12262.6478	-0.0006
	48	12262.5260	0.0008		3	12262.8382	0.0003
	49	12262.3216	0.0000		4	12263.0167	-0.0014
	50	12262.1085	-0.0007		5	12263.1882	-0.0018
	51	12261.8895	0.0015				

Supplemental Table 1 (Continued)

Branch	N''	Observed	Obs.-Cal.	Branch	N''	Observed	Obs.-Cal.
R_2	6	12263.3517	-0.0020	R_2	38	12264.1857	0.0006
	7	12263.5073	-0.0018		39	12264.0719	0.0005
	8	12263.6552	-0.0011		40	12263.9481	-0.0009
	9	12263.7944	-0.0008		41	12263.8198	0.0018
	10	12263.9256	-0.0002		42	12263.6796	0.0013
	11	12264.0460	-0.0021		43	12263.5305	0.0006
	12	12264.1597	-0.0024		44	12263.3733	0.0005
	13	12264.2679	0.0001		45	12263.2071	0.0001
	14	12264.3641	-0.0011		46	12263.0326	0.0001
	15	12264.4532	-0.0011		47	12262.8508	0.0016
	16	12264.5348	-0.0003		48	12262.6570	-0.0001
	17	12264.6063	-0.0012		49	12262.4574	0.0011
	18	12264.6714	-0.0002		50	12262.2460	-0.0006
	19	12264.7267	-0.0006		51	12262.0269	-0.0011
	20	12264.7751	0.0004		52	12261.8004	-0.0003
	21	12264.8140	0.0003		53	12261.5635	-0.0009
	22	12264.8448	0.0004		54	12261.3181	-0.0011
	23	12264.8673	0.0007		55	12261.0628	-0.0023
	24	12264.8821	0.0016		56	12260.8012	-0.0008
	25	12264.8865	0.0006		57	12260.5276	-0.0024
	26	12264.8845	0.0016		58	12260.2463	-0.0027
	27	12264.8723	0.0008		59	12259.9580	-0.0009
	28	12264.8531	0.0015		60	12259.6573	-0.0025
	29	12264.8238	0.0005	${}^{S}R_{21}$	0	12262.8812	0.0003
	30	12264.7873	0.0008		0	12262.8832	0.0001
	31	12264.7438	0.0026		1	12263.5070	0.0002
	32	12264.6878	0.0004		2	12264.1240	-0.0004
	33	12264.6260	0.0010		3	12264.7341	0.0003
	34	12264.5546	0.0004		4	12265.3376	0.0027
	35	12264.4752	0.0004		5	12265.9301	0.0024
	36	12264.3877	0.0009		6	12266.5162	0.0039
	37	12264.2896	-0.0007		7	12267.0913	0.0028

R.M.S = 0.0013 cm^{-1}

SUPPLEMENTAL TABLE II: Observed and calculated line positions of $A^2\Pi$-$X^2\Sigma^+(0,0)$ band system of ^{135}BaF

Branch	F''_1,F''-F'_1,F'	Observed - 10000	Obs-cal
$^{R}R_{12}(0)$	3.0, 2.5-4.0, 3.5	1631.2145	0.0011
	3.0, 2.5-3.0, 2.5	1631.2192	0.0005
	3.0, 2.5-2.0, 1.5	1631.2217	-0.0006
$^{R}R_{11}(0)$	2.0, 1.5-3.0, 2.5	1631.3618	0.0020
	2.0, 1.5-2.0, 1.5	1631.3646	0.0013
	2.0, 1.5-1.0, 0.5	1631.3666	0.0015
$^{R}R_{12}(1)$	3.0, 2.5-4.0, 3.5	1632.1150	-0.0015
	2.0, 1.5-3.0, 2.5	1632.1179	-0.0020
	2.0, 1.5-2.0, 1.5	1632.1200	-0.0022
$^{R}R_{11}(1)$	4.0, 3.5-5.0, 4.5	1632.8635	-0.0017
	2.0, 1.5-3.0, 2.5	1632.8660	-0.0016
	3.0, 2.5-3.0, 2.5	1632.8690	-0.0018
$^{R}R_{12}(4)$	7.0, 6.5-8.0, 7.5	1634.1865	0.0022
	6.0, 5.5-7.0, 6.5	1634.1931	0.0003
	5.0, 4.5-6.0, 5.5	1634.2012	0.0016
	4.0, 3.5-5.0, 4.5	1634.2078	0.0027
$^{R}R_{11}(4)$	4.0, 3.5-5.0, 4.5	1634.3368	0.0002
	5.0, 4.5-6.0, 5.5	1634.3375	-0.0010
$^{R}R_{12}(7)$	9.0, 8.5-10.0, 9.5	1636.3244	0.0018
	9.0, 8.5-10.0, 9.5	1636.3306	-0.0009
	8.0, 7.5-9.0, 8.5	1636.3381	-0.0021
	7.0, 6.5-8.0, 7.5	1636.3455	-0.0025
$^{R}R_{11}(7)$	7.0, 6.5-8.0, 7.5	1636.4785	0.0022
	8.0, 7.5-9.0, 8.5	1636.4808	0.0007
$^{O}P_{12}(7)$	9.0, 8.5-8.0, 7.5	1624.8484	-0.0001
	8.0, 7.5-7.0, 6.5	1624.8498	-0.0002
	7.0, 6.5-6.0, 5.5	1624.8516	0.0000
	6.0, 5.5-5.0, 4.5	1624.8535	0.0001
$^{R}Q_{22}(1)$	3.0, 2.5-4.0, 3.5	2262.3838	0.0002
$^{R}Q_{21}(1)$	2.0, 1.5-2.0,1.5	2262.5233	0.0003
	3.0, 2.5-3.0, 2.5	2262.5245	0.0007
$^{R}Q_{21}(2)$	2.0, 1.5-2.0, 1.5	2262.7144	-0.0014
	4.0, 3.5-4.0, 3.5	2262.7184	-0.0020
$^{S}R_{22}(4)$	7.0, 6.5-8.0, 7.5	2265.2782	0.0004
	6.0, 5.5-7.0, 6.5	2265.2815	-0.0009
	5.0, 4.5-6.0, 5.5	2265.2865	0.0007
	4.0, 3.5-5.0, 4.5	2265.2910	0.0024
$^{S}R_{21}(4)$	4.0, 3.5-5.0, 4.5	2265.4193	-0.0007
	5.0, 4.5-6.0, 5.5	2265.4233	-0.0015
	6.0, 5.5-7.0, 6.5	2265.4263	-0.0006
$^{S}R_{22}(7)$	10.0, 9.5-11.0, 10.5	2267.0383	0.0016
	9.0, 8.5-10.0, 9.5	2267.0423	-0.0007
	8.0, 7.5-9.0, 8.5	2267.0469	-0.0015
	7.0, 6.5-8.0, 7.5	2267.0521	-0.0012
$^{S}R_{21}(7)$	7.0, 6.5-8.0, 7.5	2267.1840	0.0024

	8.0, 7.5-9.0, 8.5	2267.1880	-0.0004
	9.0, 8.5-10.0, 9.5	2267.1920	-0.0002
${}^{Q}P_{22}+{}^{Q}Q_{22}$ (2)	4.0, 3.5-4.0, 3.5	2261.5170	0.0011
${}^{Q}P_{21}+{}^{Q}Q_{21}$ (2)	4.0, 3.5-4.0, 3.5	2261.6578	0.0003
${}^{Q}P_{22}+{}^{Q}Q_{22}$ (3)	3.0, 2.5-2.0, 1.5	2261.4146	-0.0005
	4.0, 3.5-3.0, 2.5	2261.4197	0.0005
	5.0, 4.5-5.0, 4.5	2261.4228	0.0021
${}^{Q}P_{22}+{}^{Q}Q_{22}$ (4)	7.0, 6.5-6.0, 5.5	2261.0280	0.0015
	6.0, 5.5-6.0, 5.5	2261.0292	-0.0019
${}^{Q}P_{21}+{}^{Q}Q_{21}$ (4)	4.0, 3.5-3.0, 2.5	2261.1689	0.0001
	5.0, 4.5-4.0, 3.5	2261.1723	-0.0012
	6.0, 5.5-6.0, 5.5	2261.1763	0.0007
${}^{Q}P_{22}+{}^{Q}Q_{22}$ (7)	10.0, 9.5-9.0, 8.5	2260.2388	0.0037
	9.0, 8.5-9.0, 8.5	2260.2408	-0.0007
	8.0, 7.5-8.0, 7.5	2260.2454	-0.0014
	6.0, 5.5-6.0, 5.5	2260.2491	-0.0022
	7.0, 6.5-7.0, 6.5	2260.2536	0.0019
${}^{Q}P_{21}+{}^{Q}Q_{21}$ (7)	7.0, 6.5-6.0, 5.5	2260.3799	-0.0001
	8.0, 7.5-8.0, 7.5	2260.3861	-0.0007
	9.0, 8.5-9.0, 8.5	2260.3911	0.0005
${}^{Q}P_{22}+{}^{Q}Q_{22}$ (6)	8.0, 7.5-7.0, 6.5	2260.5060	-0.0023
	8.0, 7.5-8.0, 7.5	2260.5110	-0.0020
	7.0, 6.5-7.0, 6.5	2260.5160	-0.0017
	6.0, 5.5-6.0, 5.5	2260.5210	-0.0009
	5.0, 4.5-5.0, 4.5	2260.5257	0.0000
${}^{Q}P_{21}+{}^{Q}Q_{21}$ (6)	6.0, 5.5-5.0, 4.5	2260.6525	0.0013
	7.0, 6.5-7.0, 6.5	2260.6590	0.0017
	8.0, 7.5-8.0, 7.5	2260.6630	0.0024
	Sdt. Dev.= 0.00153 cm^{-1}		

All units are in wave number cm^{-1}.

SUPPLEMENTAL TABLE III. Observed and calculated line positions of $A^2\Pi$-$X^2\Sigma^+(0,0)$ band system of ^{137}BaF

Branch	$F''_1,F''-F'_1,F'$	Observed - 10000	Obs-cal
$^{R}R_{12}(4)$	7.0, 6.5-8.0, 7.5	1634.1865	0.0030
	6.0, 5.5-7.0, 6.5	1634.1931	0.0004
	5.0, 4.5-6.0, 5.5	1634.2012	0.0012
	4.0, 3.5-5.0, 4.5	1634.2078	0.0019
$^{R}R_{11}(4)$	4.0, 3.5-5.0, 4.5	1634.3518	-0.0005
	5.0, 4.5-6.0, 5.5	1634.3525	-0.0015
$^{O}P_{12}(7)$	6.0, 5.5-5.0, 4.5	1624.8673	-0.0015
	6.0, 5.5-5.0, 4.5	1624.8691	-0.0014
$^{O}P_{11}(7)$	8.0, 7.5-7.0, 6.5	1625.0221	-0.0010
	9.0, 8.5-8.0, 7.5	1625.0286	-0.0027
$^{O}P_{12}(10)$	12.0, 11.5-11.0, 10.5	1622.3420	0.0018
	11.0, 10.5-10.0, 9.5	1622.3430	-0.0002
	10.0, 9.5-9.0, 8.5	1622.3453	-0.0009
	8.0, 7.5-7.0, 6.5	1622.3482	-0.0007
	9.0, 8.5-8.0, 7.5	1622.3496	-0.0004
	10.0, 9.5-9.0, 8.5	1622.4894	0.0029
$^{O}P_{11}(10)$	11.0, 10.5-10.0, 9.5	1622.5008	0.0015
	12.0, 11.5-11.0, 10.5	1622.5089	-0.0001
$^{R}R_{12}(1)$	4.0, 3.5-5.0,4.5	1631.9721	0.0005
	3.0, 2.5-4.0,3.5	1631.9736	0.0008
	3.0, 2.5-4.0, 3.5	1631.9784	-0.0013
	2.0, 1.5-3.0, 2.5	1631.9803	-0.0006
$^{R}R_{11}(1)$	3.0, 2.5-4.0, 3.5	1632.1338	-0.0010
	2.0, 1.5-3.0,2.5	1632.1371	-0.0018
	2.0, 1.5-2.0, 1.5	1632.1400	-0.0016
$^{Q}P_{22}+^{Q}Q_{22}$ (7)	6.0, 5.5-6.0, 5.5	2260.2697	0.0001
	7.0, 6.5-7.0, 6.5	2260.2646	-0.0005
	8.0, 7.5-8.0, 7.5	2260.2600	-0.0003
	9.0, 8.5-9.0, 8.5	2260.2548	-0.0001
	10.0, 9.5-9.0, 8.5	2260.2502	0.0017
$^{Q}P_{21}+^{Q}Q_{21}$ (7)	9.0, 8.5-9.0, 8.5	2260.4196	0.0007
	8.0, 7.5-8.0, 7.5	2260.4149	-0.0003
	7.0, 6.5-6.0, 5.5	2260.4088	0.0006
$^{Q}P_{22}+^{Q}Q_{22}$ (8)	5.0, 4.5-5.0, 4.5	2260.5373	-0.0006
	6.0, 5.5-6.0, 5.5	2260.5333	-0.0008
	7.0, 6.5-7.0, 6.5	2260.5293	-0.0007
	8.0, 7.5-8.0, 7.5	2260.5257	0.0004
	8.0, 7.5-7.0, 6.5	2260.5210	0.0005
$^{Q}P_{21}+^{Q}Q_{21}$ (8)	8.0, 7.5-8.0, 7.5	2260.6888	0.0011
	7.0, 6.5-7.0, 6.5	2260.6848	0.0002
	6.0, 5.5-5.0, 4.5	2260.6783	0.0000
$^{R}Q_{22}+^{R}R_{22}$ (1)	3.0, 2.5-4.0, 3.5	2262.3893	-0.0004
$^{R}Q_{21}+^{R}R_{21}$ (1)	3.0, 2.5-3.0, 2.5	2262.5425	-0.0024
$^{Q}P_{22}+^{Q}Q_{22}$ (3)	6.0, 5.5-5.0, 4.5	2261.2820	-0.0009
	5.0, 4.5-5.0, 4.5	2261.2851	-0.0019

	4.0, 3.5-4.0, 3.5	2261.2882	-0.0016
	3.0, 2.5-3.0, 2.5	2261.2906	-0.0011
$^{Q}P_{22}+{}^{Q}Q_{22}$ (4)	7.0, 6.5-6.0, 5.5	2261.0375	0.0009
	6.0, 5.5-6.0, 5.5	2261.0422	0.0009
	5.0, 4.5-5.0, 4.5	2261.0443	-0.0005
	4.0, 3.5-4.0, 3.5	2261.0455	-0.0020
	3.0, 2.5-3.0, 2.5	2261.0467	-0.0029
$^{O}P_{12}(4)$	2.0, 1.5-1.0, 0.5	1627.3119	-0.0008
	4.0, 3.5-3.0, 2.5	1627.3143	0.0000
	5.0, 4.5-4.0, 3.5	1627.3162	0.0007
	6.0, 5.5-5.0, 4.5	1627.3191	0.0018
$^{R}R_{12}(7)$	10.0- 9.5-11.0, 10.5	1636.3194	0.0013
	9.0, 8.5-10.0, 9.5	1636.3281	-0.0007
	8.0, 7.5-9.0, 8.5	1636.3372	-0.0009
	7.0, 6.5-8.0, 7.5	1636.3463	0.0000
$^{R}R_{11}(7)$	7.0, 6.5-8.0, 7.5	1636.4902	0.0008
	8.0, 7.5-9.0, 8.5	1636.4921	-0.0008
$^{S}R_{22}(4)$	7.0, 6.5-8.0, 7.5	2265.2782	0.0013
	6.0, 5.5-7.0, 6.5	2265.2815	-0.0001
	5.0, 4.5-6.0, 5.5	2265.2865	0.0014
	4.0, 3.5-5.0, 4.5	2265.2910	0.0032
$^{S}R_{21}(4)$	4.0, 3.5-5.0, 4.5	2265.4368	0.0027
	5.0, 4.5-6.0, 5.5	2265.4404	0.0013
	6.0, 5.5-7.0, 6.5	2265.4428	0.0018
$^{S}R_{22}(7)$	10.0, 9.5-11.0, 10.5	2267.0346	0.0022
	9.0, 8.5-10.0, 9.5	2267.0396	0.0007
	8.0, 7.5-9.0, 8.5	2267.0446	0.0003
	7.0, 6.5-8.0, 7.5	2267.0493	0.0002
$^{S}R_{21}(7)$	7.0, 6.5-8.0, 7.5	2267.1947	0.0025
	8.0, 7.5-9.0, 8.5	2267.1997	0.0005
	9.0, 8.5-10.0, 9.5	2267.2047	0.0019
$^{S}R_{22}(10)$	13.0, 12.5-14.0, 13.5	2268.7139	0.0006
	12.0, 11.5-13.0, 12.5	2268.7190	-0.0023
	11.0, 10.5-12.0, 11.5	2268.7202	-0.0018
	11.0, 10.5-12.0, 11.5	2268.7265	-0.0020
	10.0, 9.5-11.0, 10.5	2268.7277	-0.0011
	10.0, 9.5-11.0, 10.5	2268.7340	-0.0014
$^{R}R_{12}(0)$	3.0, 2.5-4.0, 3.5	1631.2192	0.0018
	3.0, 2.5-3.0,2.5	1631.2242	0.0006
	3.0, 2.5-2.0,1.5	1631.2272	-0.0005
$^{R}R_{11}(0)$	2.0, 1.5-3.0,2.5	1631.3816	0.0020
	2.0,1.5-2.0,1.5	1631.3863	0.0026
	2.0,1.5-1.0, 0.5	1631.3875	0.0018
$^{R}R_{12}(2)$	5.0, 4.5-6.0, 5.5	1632.7155	-0.0019
	4.0, 3.5-5.0, 4.5	1632.7258	0.0000
	3.0, 2.5-4.0, 3.5	1632.7296	-0.0021
$^{R}R_{11}(2)$	4.0, 3.5-5.0, 4.5	1632.8811	-0.0012
	2.0, 1.5-3.0, 2.5	1632.8851	-0.0002
	3.0, 2.5-3.0, 2.5	1632.8878	-0.0010
$^{R}Q_{22}+{}^{R}R_{22}$ (2)	4.0, 3.5-5.0, 4.5	2262.5856	0.0010

${}^{R}Q_{21}+{}^{R}R_{21}$ (2)	2.0, 1.5-2.0, 1.5	2262.7347	-0.0018
	4.0, 3.5-4.0, 3.5	2262.7387	-0.0024
${}^{Q}P_{22}+{}^{Q}Q_{22}$ (2)	4.0, 3.5-4.0, 3.5	2261.5249	0.0004
${}^{Q}P_{21}+{}^{Q}Q_{21}$ (2)	4.0, 3.5-3.0, 2.5	2261.6815	0.0006
	Std. dev= 0.00144cm^{-1}		

All units are in wave number cm^{-1}.

Table I. The observed and calculated Stark shifts for the $A^2\Pi$-$X^2\Sigma^+$(0,0) band system of ^{138}BaF.

Branch, Pol	Field (V/cm)	Assign[a]	Shift (MHz)	Obs-Calc[b]
P_{12} (2), ||	806.3	A	-25	-9
	1611.9	A	-64	-1
	1741.5	A	-79	-7
		B	-78	-8
	2014.0	A	-103	-7
		B	-89	3
	2341.5	A	-127	2
		B	-128	-2
	2416.0	A	-136	1
		B	-125	8
	2940.9	A	-207	-4
		B	-194	2
	3540.9	A	-292	4
		B	-281	2
		Std. dev.=5.5 MHz		
$^SR_{21}$(0), ⊥	600.9	D	259	-1
	600.9	C	93	-8
	600.9	B	-66	-10
	600.9	A	-223	-9
	899.4	D	412	5.7
	899.4	C	172.8	3.4
	899.4	B	-69.7	-2.6
	899.4	A	-307.9	-4.8
	1201.5	D	549.3	-17.3
	1201.5	C	239.2	-10.0
	1201.5	B	-376.2	6.0
	1501.2	B	-67.1	-11.3
	1501.2	A	-439.2	9.9
	1742.1	D	887.0	7.2
	1742.1	C	415.7	-3.7
	1742.1	B	-47.2	-8.3
	1742.1	A	-500.2	-5.2
		Std. dev.=8.4 MHz		

a) Refers to transitions indicated in Figures 6 and 7.

b) Calculated shifts obtained using optimized μ_e of 1.50(2) D and 1.31(2) D for the $A^2\Pi_{1/2}$(υ=0) and $A^2\Pi_{3/2}$ (υ=0) states and previously determined μ_e of 3.170(3)D for the $X^2\Sigma^+$(v =0) state [12].

Table II. The observed and calculated Zeeman shifts for the $A^2\Pi$-$X^2\Sigma^+$(0,0) band system of ^{138}BaF.

Branch	Field (Gauss)	M_J'	M_J''	Obs (MHz)	Dif (MHz)	Branch	Field (Gauss)	M_J'	M_J''	Obs (MHz)	Dif (MHz)
$R_1(0)$	948	1/2	1/2	-1387	26	$R_1(0)$	250	3/2	1/2	-402	21
$\parallel$	948	-1/2	-1/2	1408	-3	$\perp$	250	-1/2	1/2	-297	25
	931	1/2	1/2	-1442	-54		250	1/2	-1/2	331	10
	931	-1/2	-1/2	1419	33		250	-3/2	-1/2	423	0
	833	1/2	1/2	-1227	14	$^SR_{21}(0)$	137	1/2	1/2	-111	4
	833	-1/2	-1/2	1243	3	$\parallel$	137	-1/2	-1/2	128	15
	713	1/2	1/2	-1127	-65		141	1/2	1/2	-106	12
	713	-1/2	-1/2	1094	33		141	-1/2	-1/2	117	0
	482	1/2	1/2	-766	-48		192	1/2	1/2	-166	-4
	482	-1/2	-1/2	742	24		192	-1/2	-1/2	172	13
	248	1/2	1/2	-412	-43		228	1/2	1/2	-183	9
	248	-1/2	-1/2	387	18		228	-1/2	-1/2	192	4
	136	1/2	1/2	-249	-46		230	1/2	1/2	-206	-12
	136	-1/2	-1/2	211	8		230	-1/2	-1/2	175	-14
$R_1(0)$	948	3/2	1/2	-1578	28		253	1/2	1/2	-207	7
$\perp$	948	-1/2	1/2	-1176	44		253	-1/2	-1/2	230	21
	948	1/2	-1/2	1211	-7		254	1/2	1/2	-226	-12
	948	-3/2	-1/2	1612	9		254	-1/2	-1/2	193	-16
	833	3/2	1/2	-1372	39		307	1/2	1/2	-244	16
	833	-1/2	1/2	-1035	37		307	-1/2	-1/2	271	19
	833	1/2	-1/2	1060	-11		310	1/2	1/2	-279	-17
	833	-3/2	-1/2	1417	8		310	-1/2	-1/2	242	-13
	724	3/2	1/2	-1214	-18	$^SR_{21}(0)$	141	-1/2	1/2	-265	10
	724	-1/2	1/2	-984	-52	$\perp$	141	1/2	-1/2	267	-6
	724	1/2	-1/2	912	19		192	-1/2	1/2	-374	1
	724	-3/2	-1/2	1207	-18		192	3/2	1/2	51	-1
	604	3/2	1/2	-1017	6		192	-3/2	-1/2	-49	5
	604	-1/2	1/2	-759	18		192	1/2	-1/2	383	11
	604	1/2	-1/2	774	-2		228	-1/2	1/2	-459	-13
	604	-3/2	-1/2	1009	-13		228	1/2	-1/2	445	4
	489	3/2	1/2	-816	12		230	-1/2	1/2	-459	-11
	489	-1/2	1/2	-612	17		230	3/2	1/2	48	-14
	489	1/2	-1/2	612	-17		230	-3/2	-1/2	-78	-14
	489	-3/2	-1/2	820	-7		254	-1/2	1/2	-517	-21
	364	3/2	1/2	-611	5		254	3/2	1/2	58	-10
	364	-1/2	1/2	-458	10		254	-3/2	-1/2	-85	-14
	364	1/2	-1/2	470	2		310	3/2	1/2	63	-20
	364	-3/2	-1/2	625	9		310	-3/2	-1/2	-107	-19

Standard deviation of fit = 21.5 MHz.

Table III. The field-free spectroscopic parameters in wave numbers (cm^{-1}) for the $A^2\Pi$-$X^2\Sigma^+$ (0,0) band system of BaF

Parameter	^{138}BaF	^{137}BaF	^{135}BaF
$X^2\Sigma^+(\upsilon=0)$			
B	0.21594802[a]	0.21613878[d]	0.21675(5)
$10^7\times D$	1.85[b]	1.85[b]	1.85[e]
γ	0.00269930[a]	0.002702703 [d]	0.00270270[e]
b_F(Ba)	NA	0.077587 [d]	0.0702(5)
c(Ba)	NA	0.0250173 [d]	0.002237381[f]
eq_0Q(Ba)	NA	-.00390270 [d]	-0.003490348 [f]
b_F(F)	0.002209862[c]	0.002209873[d]	0.002209873 [d]
c(F)	0.000274323[c]	0.000274323[d]	0.000274323 [d]
$A^2\Pi$ (υ=0)			
A	632.28175(6)	632.2802(8)	632.2803(10)
$10^5\times A_D$	3.1(2)	3.1[e]	3.1[e]
B	0.2117414(10)	2.11937(12)	0.2125(4)
$10^7\times D$	2.00[b]	2.00[b]	2.00[b]
$(p+2q)$	-0.25755(10)	-0.2581(2)	-0.25755[e]
d(Ba)	NA	0.0076(10)	0.00685[f]
T_{00}	11946.3168(2)	11945.3152(6)	11946.3034(10)
Std. Dev.	0.0013	0.0014	0.0015

[a] Ref. 10.
[b] Ref. 15.
[c] Ref. 12.
[d] Ref. 11.
[e] Constrained to value scaled from the fit of the ^{138}BaF transitions.
[f] Constrained to value obtained from scaling the value for ^{137}BaF.

Table IV. The optimized magnetic g-factors $A^2\Pi(v=0)$ and $X^2\Sigma^+(v=0)$ states of ^{138}BaF.

Parameter [a]	Value	Correlation Matrix		
$g_l'(A^2\Pi)$	-0.536(23)	1		
$g_L'(A^2\Pi)$	0.980(35)	-0.6497	1	
$g_l(X^2\Sigma^+)$	-0.028(13)	0.2233	0.2314	1

a) g_s for the $A^2\Pi(v=0)$ and $X^2\Sigma^+(v=0)$ states constrained to 2.002, $g_l(A^2\Pi)$ was set to zero.

Table V. The permanent electric dipole moments (Debye, D) for the alkaline earth monofluorides

State	CaF		SrF		BaF	
	Value	Ref.	Value	Ref.	Value	Ref.
$X^2\Sigma^+$	3.07(7)	33	3.4963(6)	35	3.170(3)	12
$A^2\Pi_{1/2}$	-	-	-		1.50(2)	present
$A^2\Pi_{3/2}$	2.45(6)	34	2.06(5)	36	1.31(2)	present

FIGURE 1

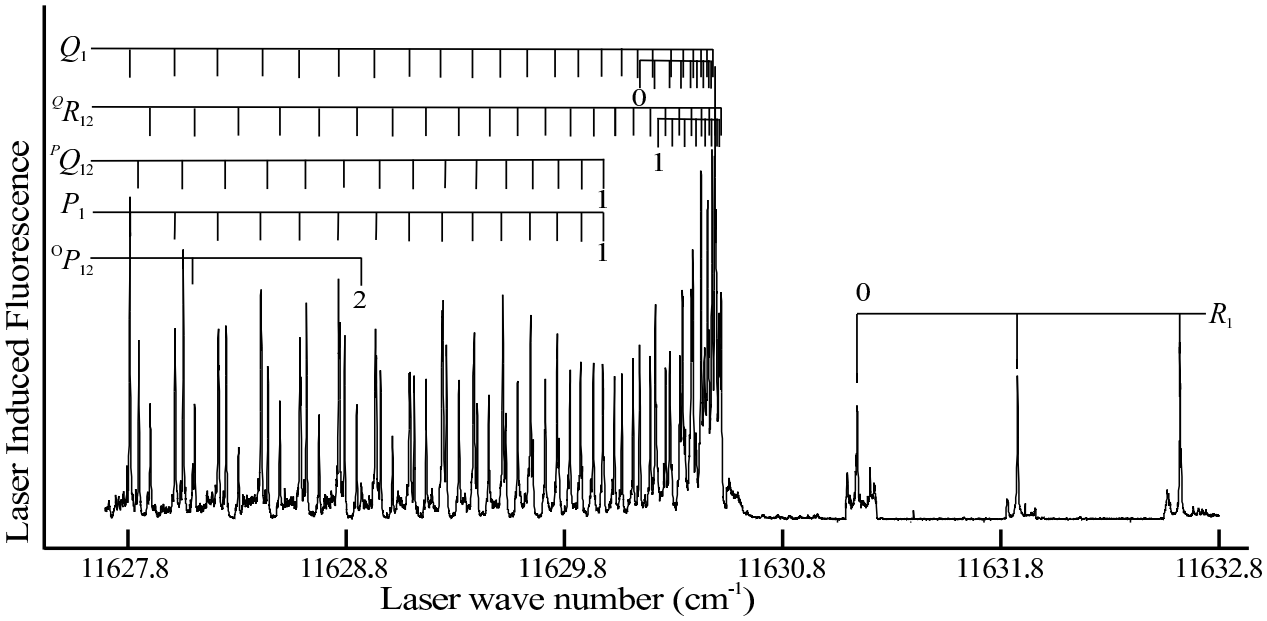

Figure 1 AD10803 27MAY2011

FIGURE 2

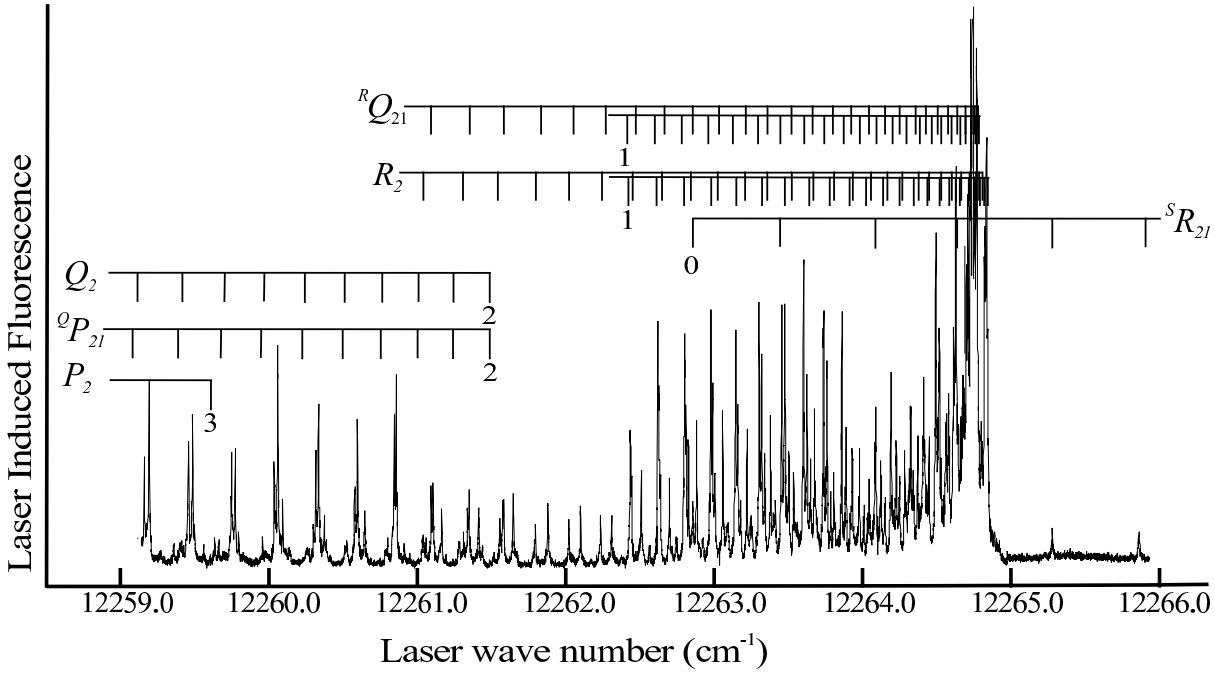

Figure 2 AD10803 27MAY2011

FIGURE 3

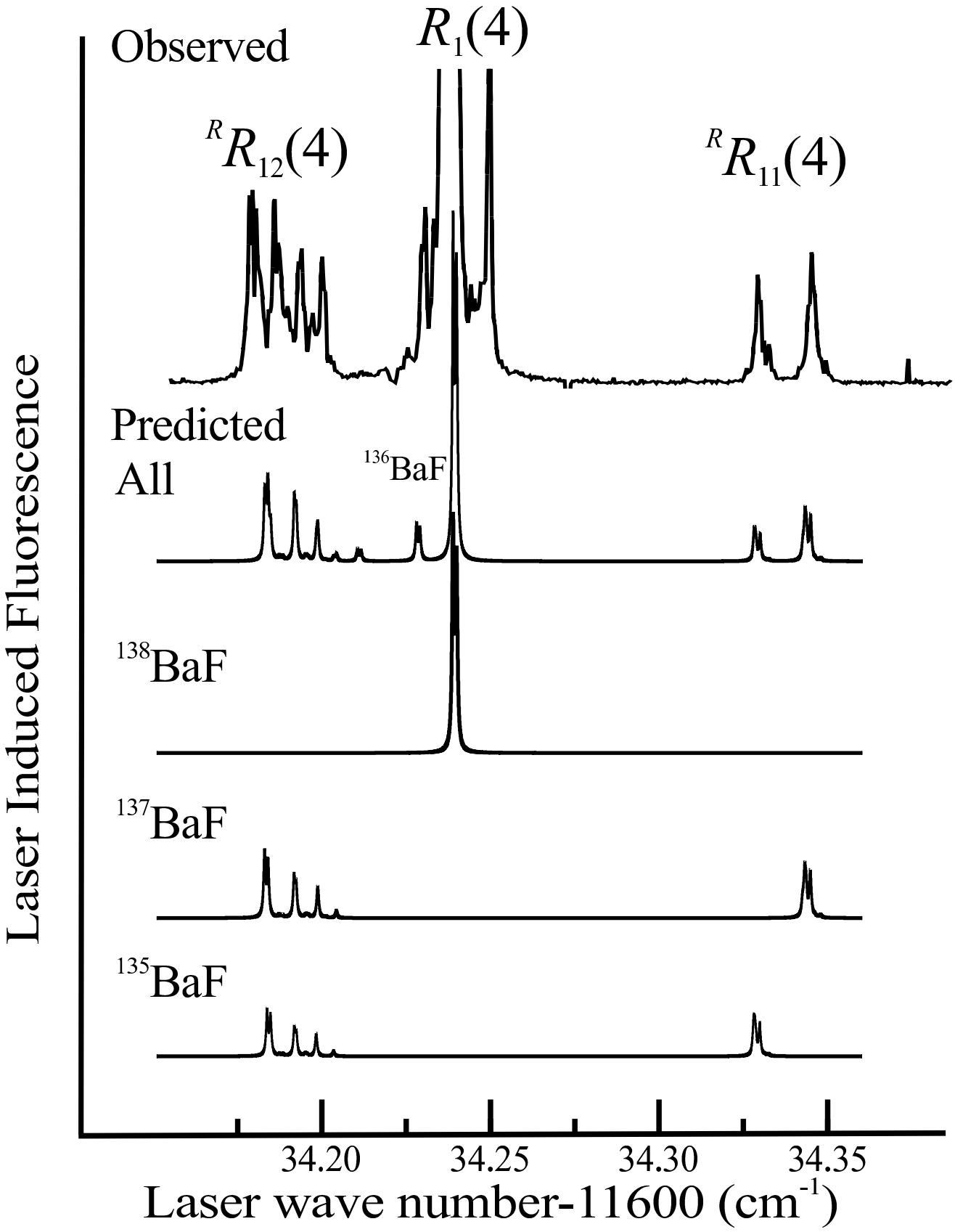

Figure 3 AD10803 27MAY2011

Figure 4

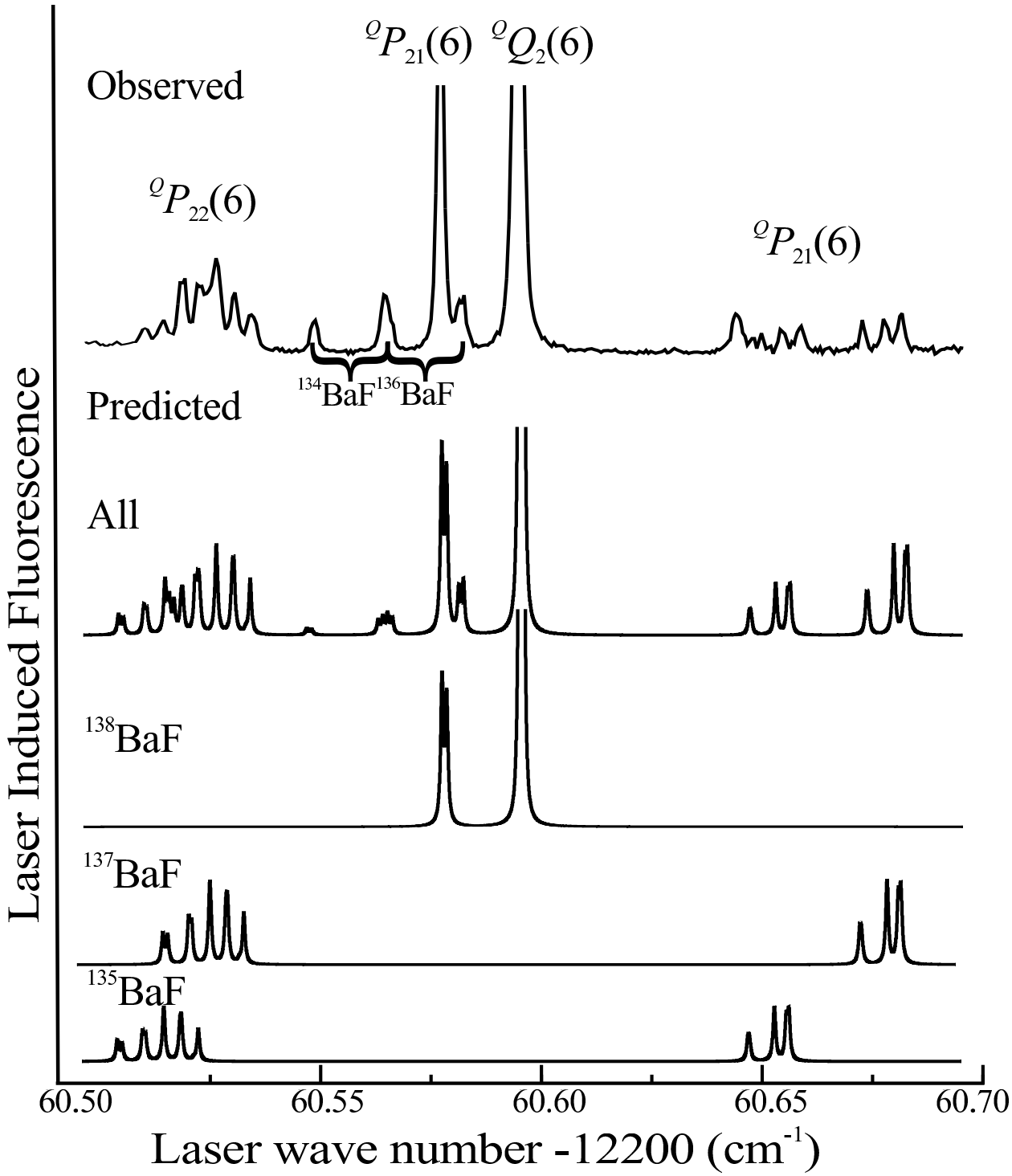

Figure 4 AD10803 27MAY2011

Figure 5

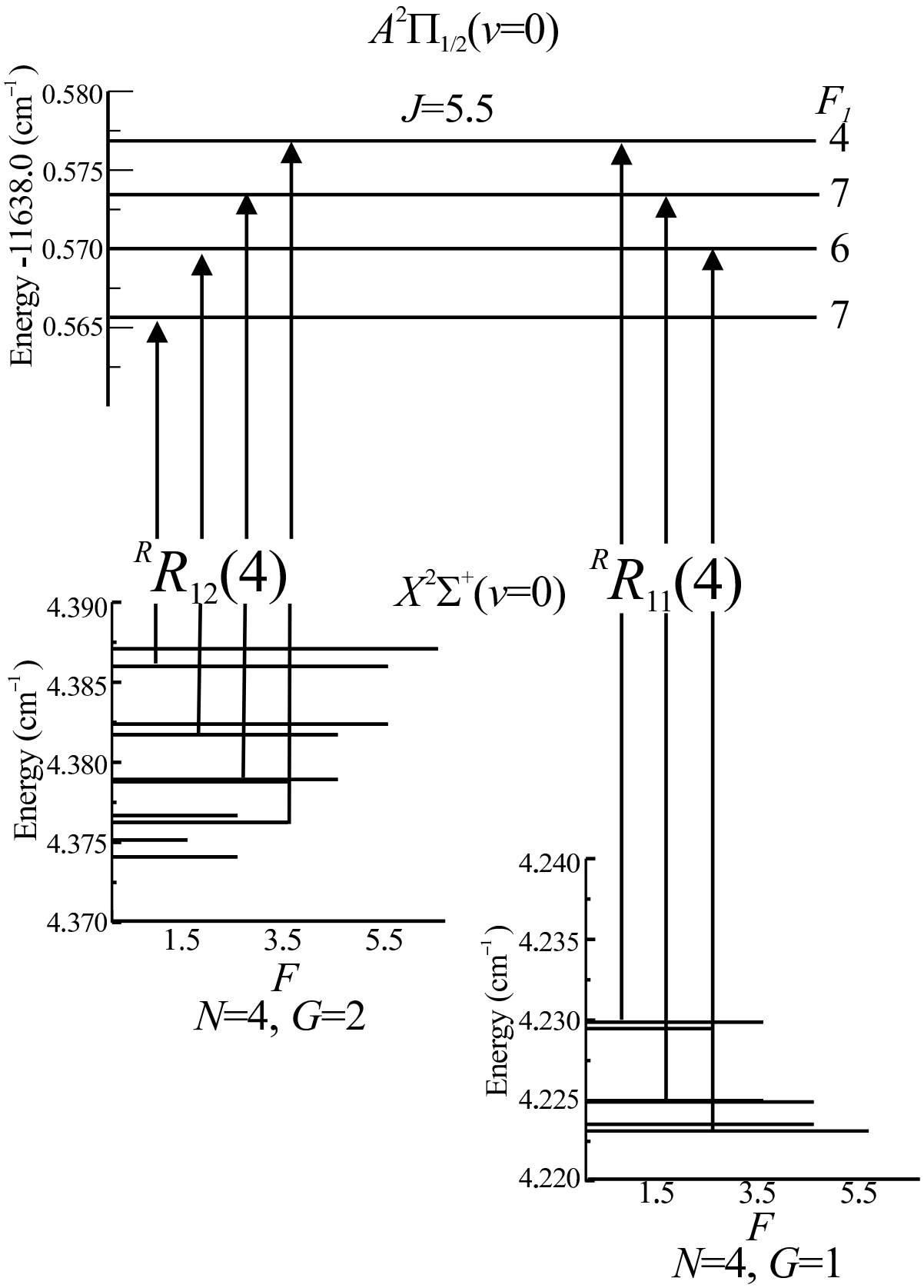

Figure 5 AD10803 27MAY2011

Figure 6

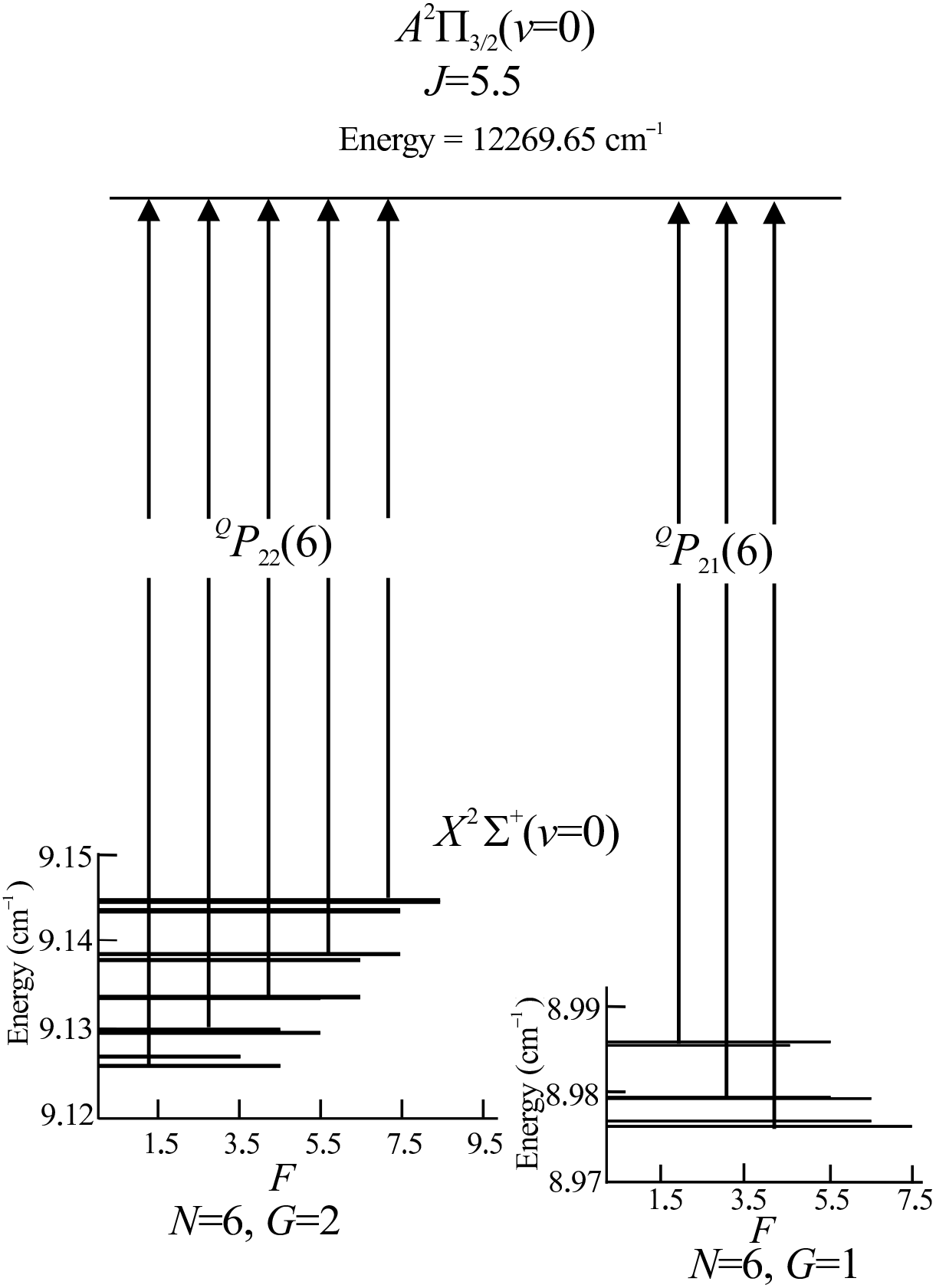

Figure 6 AD10803 27MAY2011

Figure 7

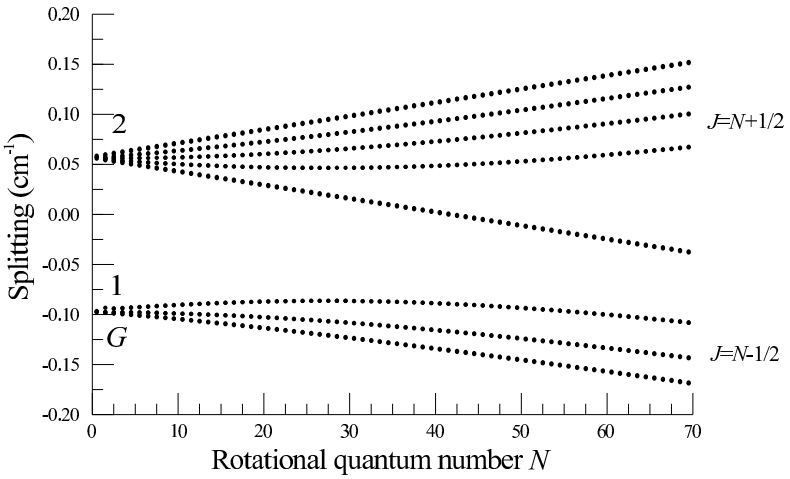

Rotational quantum number, N ⟶

Figure 7 AD10803 27MAY2011

Figure 8

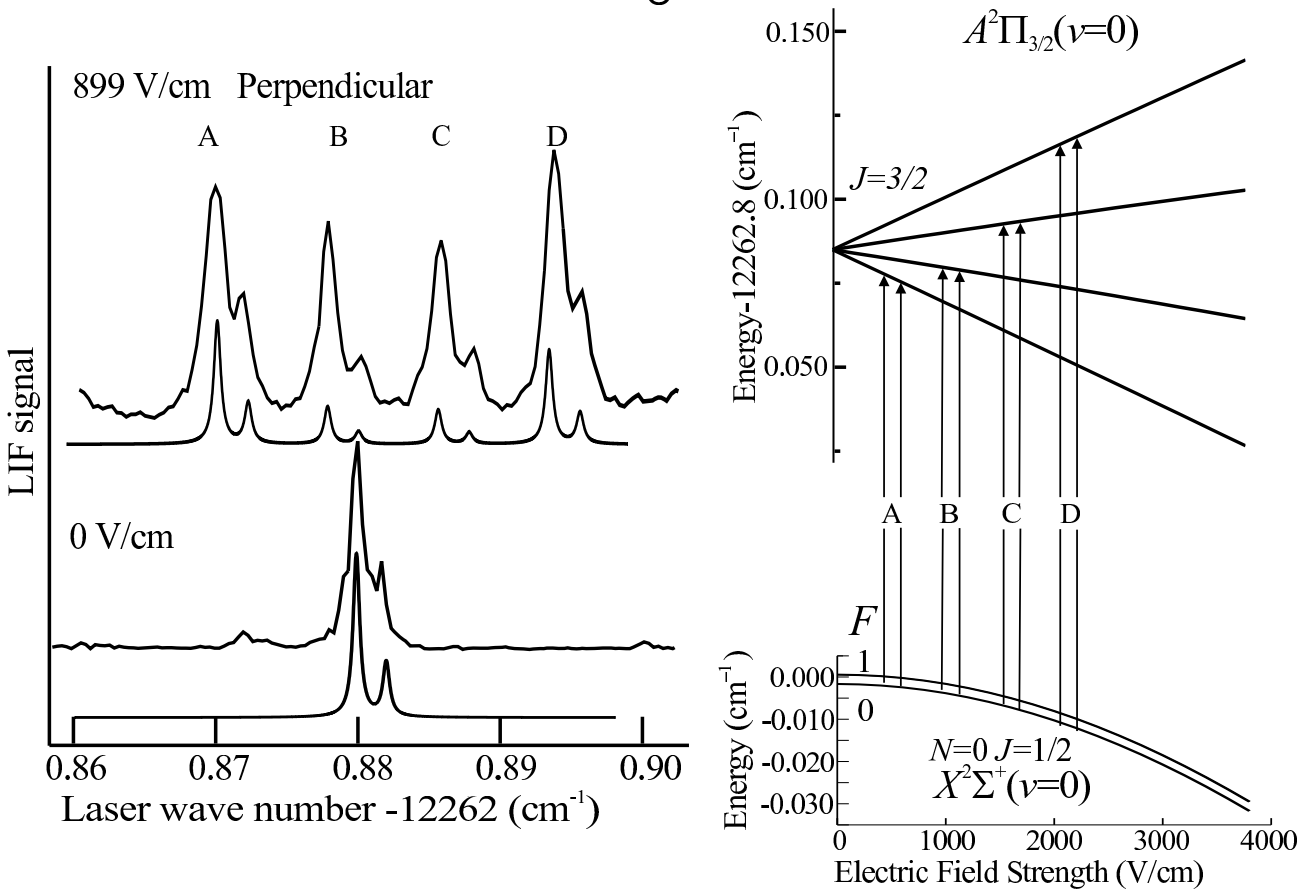

Figure 8 AD10803 27MAY2011

Figure 9

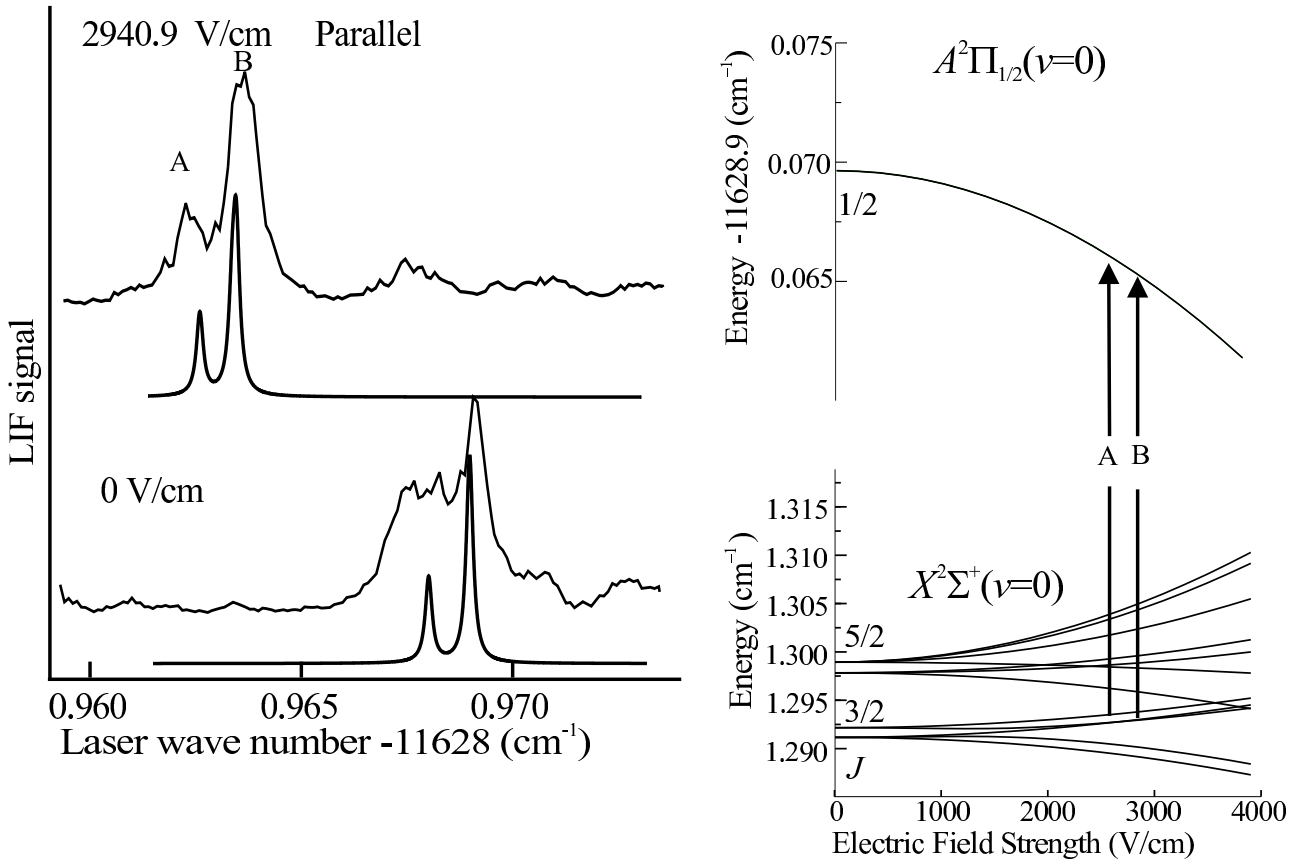

Figure 9 AD10803 27MAY2011

FIGURE 10

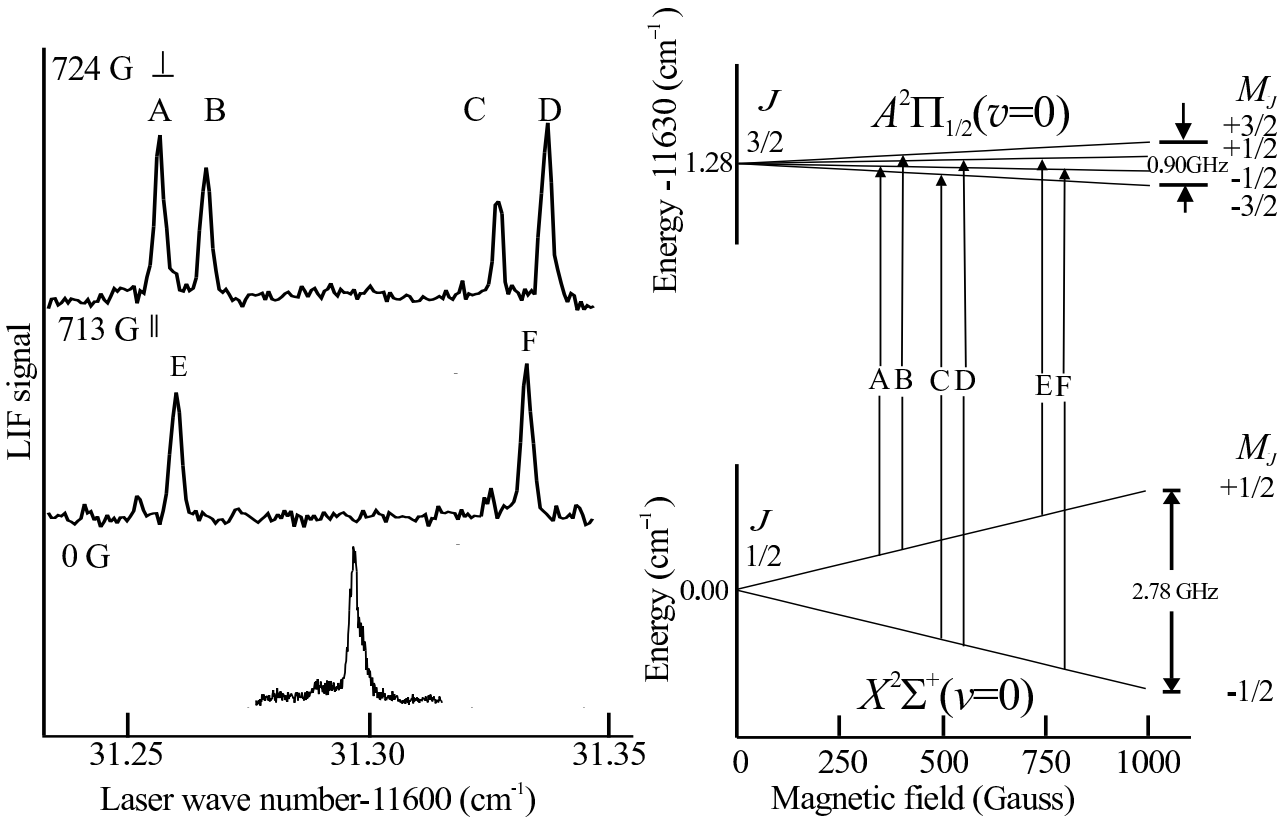

Figure 10 AD10803 27MAY2011

Figure 11

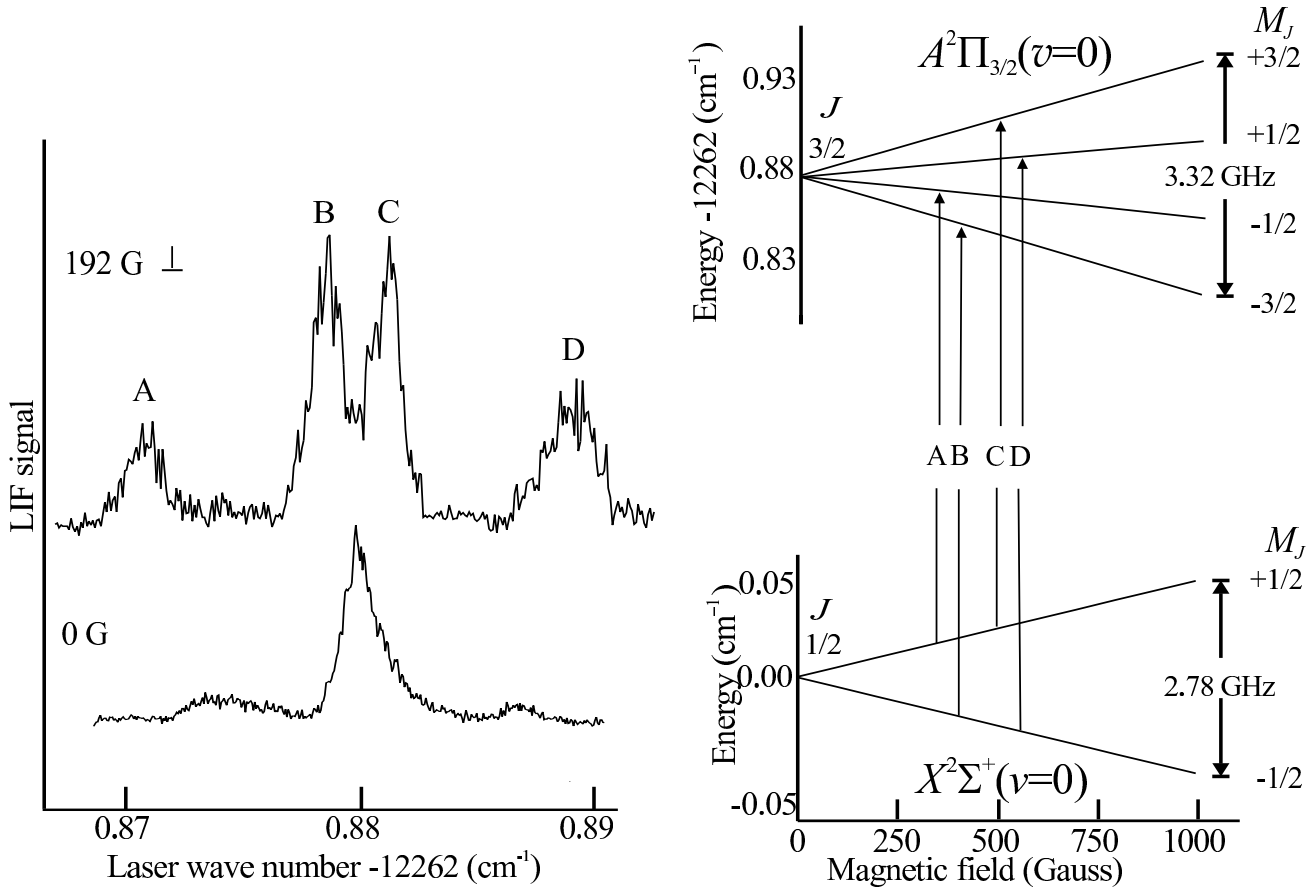
LIF signal
192 G ⊥
0 G
A
B
C
D
0.87
0.88
0.89
Laser wave number -12262 (cm-1)
Energy - 12262 (cm-1)
0.93
0.88
0.83
J
3/2
A2Π3/2(v=0)
MJ
+3/2
+1/2
3.32 GHz
-1/2
-3/2
AB CD
Energy (cm-1)
0.05
0.00
-0.05
J
1/2
2.78 GHz
X2Σ+(v=0)
0
250
500
750
1000
Magnetic field (Gauss)